Inorg. Chem. **2006**, *45*, 2989–3003

Structural, Thermodynamic, and Mesomorphic Consequences of Replacing Nitrates with Trifluoroacetate Counteranions in Ternary Lanthanide Complexes with Hexacatenar Tridentate Ligands

Homayoun Nozary,[†] Stéphane Torelli,[†] Laure Guénée,[†] Emmanuel Terazzi,[†] Gérald Bernardinelli,[§] Bertrand Donnio,[#] Daniel Guillon,[#] and Claude Piguet*[,†]

Department of Inorganic, Analytical and Applied Chemistry, University of Geneva, 30 quai E. Ansermet, CH-1211 Geneva 4, Switzerland, Laboratory of X-ray Crystallography, University of Geneva, 24 quai E. Ansermet, CH-1211 Geneva 4, Switzerland, and Institut de Physique et Chimie des Matériaux de Strasbourg-IPCMS, Groupe des Matériaux Organiques (CNRS-ULP UMR 7504), 23 rue du Loess, B.P. 43, F-67034 Strasbourg Cedex 2, France

Received November 22, 2005

The promesogenic hexacatenar tridentate ligands **L3**^{Cn} (I shape) and **L4**^{Cn} (V shape) react with trivalent lanthanide trifluoroacetates, Ln($(CF_3CO_2)_3$, to give either monometallic [Ln(**L***i*^{Cn})$(CF_3CO_2)_3$] or trifluoroacetato-bridged bimetallic [Ln(**L***i*^{Cn})$(CF_3CO_2)_3]_2$ complexes in the solid state, as exemplified by the crystal structures of [Lu(**L4**^{C0})$(CF_3CO_2)_3$-(H_2O)], [Lu(**L4**^{C0})$(CF_3CO_2)_3]_2$, and [La(**L3**^{C4})$(CF_3CO_2)_3]_2$. Although the dimerization process is influenced by the competiting complexation of anions or solvent molecules, the coordination of $CF_3CO_2^-$ instead of NO_3^- to Ln(III) produces a significant lengthening of the Ln–N(ligand) bond distances. This translates into a considerable decrease of the affinity of the **L***i*^{C12} ($i = 3$, 4) ligands for Ln$(CF_3CO_2)_3$ in solution, thus leading to significant dissociation of the [Ln(**L***i*^{C12})$(CF_3CO_2)_3$] complexes at millimolar concentrations. The thermal properties of these complexes also suffer from their limited thermodynamic stability, and the thermotropic liquid crystalline phases produced at high temperatures reflect mixtures of different species. However, a hexagonal columnar organization characterizes the main component in the mesophases obtained with [Ln(**L3**^{C12})$(CF_3CO_2)_3$] at high temperature. A tentative interpretation of the small-angle X-ray scaterring (SAXS) profiles suggests that disklike dimers of [Ln(**L3**^{C12})$(CF_3CO_2)_3]_2$ are packed along the columnar axes. For [Ln(**L4**^{C12})$(CF_3CO_2)_3$], SAXS profiles are compatible with a lamellar organization in the mesophases originating from the existence of rodlike dimers of [Ln(**L4**^{C12})$(CF_3CO_2)_3]_2$ as the major component in the liquid-crystal state.

Introduction

Driven by the attractive magnetic and optical properties resulting from the introduction of open-shell 3d- and 4f-block metals in mesophases,[1] much effort has been focused on the design of thermotropic metallomesogens, metal-containing liquid crystals.[2] However, the considerable three-dimensional expansion brought by multivalent metal ions severely limits the preparation of complexes displaying large rodlike or disklike anisometries compatible with mesomorphic properties. In this context, six-coordinate Mn(I) and Re(I) centers coordinated to rodlike carbene−imine[3] or diimine[4] ligands remain rare examples of mesomorphic octahedral complexes producing nematic and smectic mesomorphism. The concomitant observation that an increase of the curvature of the interface separating the flexible and rigid parts in metallomesogens may help to overcome the deleterious effect of three-dimensional expansion on mesomorphic properties,[5]

* To whom correspondence should be addressed. E-mail: Claude.Piguet@chiam.unige.ch.
[†] Department of Inorganic Chemistry, University of Geneva.
[§] Laboratory of X-ray Crystallography, University of Geneva.
[#] Institut de Physique et Chimie des Matériaux de Strasbourg-IPCMS.

(1) Bruce, D. W. *J. Chem. Soc., Dalton Trans.* **1993**, 2983.
(2) (a) Serrano, J. L. *Metallomesogens, Synthesis, Properties and Applications*, VCH: Weinheim, Germany, 1996. (b) Donnio, B.; Bruce, D. W. *Struct. Bond.* **1999**, *95*, 194. (c) Donnio, B.; Guillon, D.; Deschenaux, R.; Bruce, D. W. In *Comprehensive Coordination Chemistry*; McCleverty, J. A., Meyer, T. J., Eds.; Elsevier: Oxford, U.K., 2003; Vol. 7, Chapter 79, p 357.
(3) (a) Bruce, D. W.; Liu, X. H. *Liq. Cryst.* **1995**, *18*, 165. (b) Liu, X.-H.; Abser, M. N.; Bruce, D. W. J. *Organomet. Chem.* **1998**, *551*, 271.
(4) (a) Rowe, K. E.; Bruce, D. W. J. *Chem. Soc., Dalton Trans.* **1996**, 3913. (b) Morrone, S.; Guillon, D.; Bruce, D. W. *Inorg. Chem.* **1996**, *35*, 7041.

10.1021/ic052017u CCC: $33.50 © 2006 American Chemical Society
Published on Web 03/08/2006

leads to the successful incorporation of pseudo-octahedral [M(β-diketonate)$_3$] complexes (M = Cr(III), Mn(III), Fe(III))[6] and nine-coordinate trivalent lanthanides, Ln(III),[7−9] in thermotropic mesophases. Polycatenar ligands, receptors possessing a central rigid core decorated with a large number ($m \geq 4$) of divergent flexible alkyl residues, play a crucial role in this domain because the considerable entropy release accompanying the melting of the alkyl chains compensates for the intermolecular enthalpic cohesion provided by the charged and polarizable metal-containing cores. Thermotropic mesophases are thus obtained at accessible temperatures,[10] and the large ratio of the volumes of the two incompatible parts, $V_{\text{alkylchain}}/V_{\text{rigidcore}}$, found in polycatenar complexes usually favors the formation of columnar and cubic mesomorphisms.[11] The beneficial effect produced by the increase of the $V_{\text{alkyl chain}}/V_{\text{rigid core}}$ ratio on the induction of thermotropic mesomorphism is illustrated for Ln(III) embedded in the sandwich complexes [Ln(**L1**-2H)$_2$] made up of two phthalocyanine platforms decorated with eight alkyl residues,[12] or for the trimetallic bis(hexacatenar) tabular

Chart 1

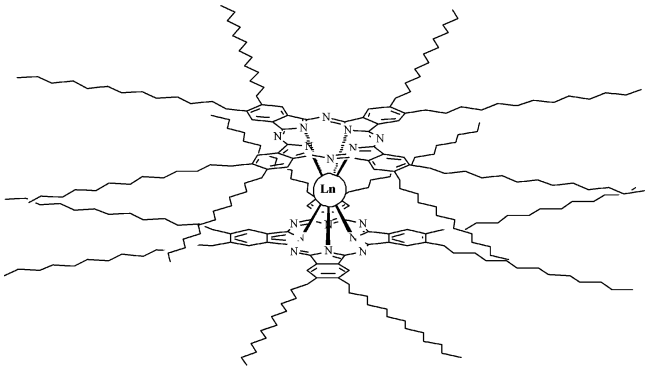

[Ln(**L1**-2H)$_2$]

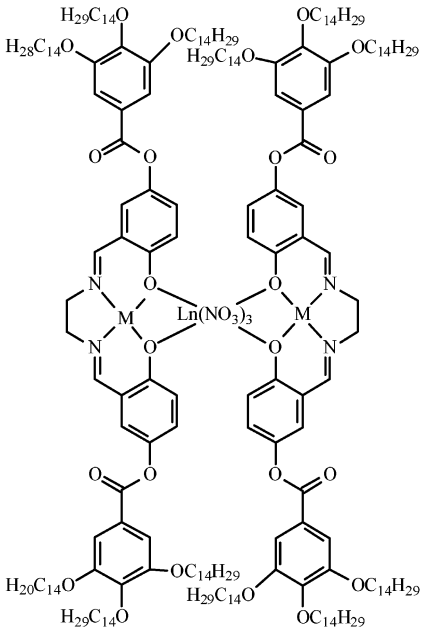

{[M(**L2**-2H)]$_2$Ln(NO$_3$)$_3$}

Schiff bases {[M(**L2**-2H)]$_2$Ln(NO$_3$)$_3$} (M = Ni(II), Cu(II)),[9] both types of complexes display hexagonal columnar mesophases at "low" temperatures (melting temperatures in the range of 20−95 °C, Chart 1). A recent thorough reexamination of the mesophases obtained with [Ln(**L1**-2H)$_2$] along the lanthanide series (Ln = Pr−Lu) shows that the size of the metals does not significantly affect the transition temperatures, which is strong support for the existence of an entropically driven melting process combined with an efficient protection of the coordinated metals by the two planar macrocyclic units.[13]

Inspired by these results, we argue that slightly reduced protection of the Ln(III)-containing core within the hexacatenar complexes [Ln(**L3**^{C12})(NO$_3$)$_3$] (V shape, Figure 1a) and [Ln(**L4**^{C12})(NO$_3$)$_3$] (I shape, Figure 1b) could provide size-dependent mesomorphism along the lanthanide series.[14] For

(5) (a) Guillon, D. *Struct. Bond*. **1999**, *95*, 41. (b) Donnio, B.; Heinrich, B.; Gulik-Krzywicki, T.; Delacroix, H.; Guillon, D.; Bruce, D. W. *Chem. Mater*. **1997**, *9*, 2951. (c) Donnio, B.; Bruce, D. W. *J. Mater. Chem*. **1998**, 1993. (d) Donnio, B.; Bruce, D. *New J. Chem*. **1999**, 275. (e) Fazio, D.; Mongin, C.; Donnio, B.; Galerne, Y.; Guillon, D., Bruce, D. W. *J. Mater. Chem*. **2001**, *11*, 2852. (f) Date, R. W.; Fernandez Iglesias, E.; Rowe, K. E.; Elliott, J. M.; Bruce, D. W. *Dalton Trans*. **2003**, 1914.

(6) (a) Zheng, H.; Swager, T. M. *J. Am. Chem. Soc*. **1994**, *116*, 761. (b) Swager, T. M.; Zheng, H. *Mol. Cryst. Liq. Cryst*. **1995**, *260*, 301.

(7) (a) Piechocki, C.; Simon, J.; André, J. J.; Guillon, D.; Petit, P.; Skoulios, A.; Weber, P. *Chem. Phys. Lett*. **1985**, *122*, 124. (b) Galyametdinov, Y.; Athanassopoulou, M. A.; Griesar, K.; Kharitonova, O.; Soto Bustamante, E. A.; Tinchurina, L.; Ovchinnikov, I.; Haase, W. *Chem. Mater*. **1996**, *8*, 922. (c) Binnemans, K.; Galymetdinov, Y. G.; Collinson, S. R.; Bruce, D. W. *J. Mater. Chem*. **1998**, *8*, 1551. (d) Miwa, H.; Kobayashi, N.; Ban, K.; Ohta, K. *Bull. Chem. Soc. Jpn*. **1999**, *72*, 2719. (e) Binnemans, K.; Galyametdinov, Y. G.; Van Deun, R.; Bruce, D. W.; Collinson, S. R.; Polishchuk, A. P.; Bikchantaev, I.; Haase, W.; Prosvirin, A. V.; Tinchurina, L.; Litvinov, U.; Gubajdullin, A.; Rakhmatullin, A.; Uytterhoeven, K.; Van Meervelt, L. *J. Am. Chem. Soc*. **2000**, *122*, 4335. (f) Martin, F.; Collinson, S. R.; Bruce, D. W. *Liq. Cryst*. **2000**, *27*, 859. (g) van Deun, R.; Binnemans, K. *Liq. Cryst*. **2001**, *28*, 621. (h) Galyametdinov, Y. G.; Haase, W.; Malykhina, L.; Prosvirin, A.; Bikchantaev, I.; Rakhmatullin, A.; Binnemans, K. *Chem.—Eur. J*. **2001**, *7*, 99. (i) Binnemans, K.; Moors, D.; Parac-Vogt, T. N.; van Deun, R.; Hinz-Hübner, D.; Meyer, G. *Liq. Cryst*. **2002**, *29*, 1209.

(8) Binnemans, K.; Görller-Walrand, C. *Chem. Rev*. **2002**, *102*, 2303.

(9) (a) Binnemans, K.; Lodewyckx, K.; Donnio, B.; Guillon, D. *Chem.—Eur. J*. **2002**, *8*, 1101. (b) Binnemans, K.; Lodewyckx, K. *Supramol. Chem*. **2003**, *15*, 485. (c) Binnemans, K.; Lodewyckx, K.; Donnio, B.; Guillon, D. *Eur.—J. Inorg. Chem*. **2005**, 1506.

(10) (a) Ziessel, R. *Coord. Chem. Rev*. **2001**, *216−217*, 195. (b) Douce, L.; Ziessel, R. *Mol. Cryst. Liq. Cryst*. **2001**, *362*, 133. (c) Donnio, B.; Heinrich, B.; Allouchi, H.; Kain, J.; Diele, S.; Guillon, D.; Bruce, D. W. *J. Am. Chem. Soc*. **2004**, *126*, 15258. (d) Terazzi, E.; Suarez, S.; Torelli, S.; Nozary, H.; Imbert, D.; Mamula, O.; Rivera, J.-P.; Guillet, E.; Bénech, J.-M. Bernardinelli, G.; Scopelliti, R.; Donnio, B.; Guillon, D.; Bünzli, J.-C. G.; Piguet, C. *Adv. Funct. Mater*. **2006**, *16*, 157.

(11) (a) Fang, Y.; Levelut, A. M.; Destrade, C. *Liq. Cryst*. **1990**, *7*, 265. (b) Malthête, J.; Nguyen, H.-T.; Destrade, C. *Liq. Cryst*. **1993**, *13*, 171. (c) Nguyen, H.-T.; Destrade, C.; Malthête, J. *Adv. Mater*. **1997**, *9*, 375. (d) Borisch, K.; Diele, S.; Göring, P.; Tschierske, C. *Liq. Cryst*. **1997**, *14*, 427. (e) Yang, D.; Armitage, B.; Marder, S. R. *Angew. Chem., Int. Ed*. **2004**, *43*, 4402.

(12) (a) Komatsu, T.; Ohta, K.; Fujimoto, T.; Yamamoto, I. *J. Mater. Chem*. **1994**, *4*, 533. (b) Toupance, T.; Bassoul, P.; Mineau, L.; Simon, J. *J. Phys. Chem*. **1996**, *100*, 11704. (c) Ban, K.; Nishizawa, K.; Ohta, K.; van de Craats, A.; Warman, J. M.; Yamamoto, I.; Shirai, H. *J. Mater. Chem*. **2001**, *11*, 321. (d) Maeda, F.; Hatsusaka, K.; Ohta, K.; Kimura, M. *J. Mater. Chem*. **2003**, *13*, 243.

(13) (a) Sleven, J.; Görller-Walrand, C.; Binnemans, K. *Mater. Sci. Eng. C* **2001**, *C18*, 229. (b) Binnemans, K.; Sleven, J.; De Feyter, S.; De Schryver, F. C.; Donnio, B.; Guillon, D. *Chem. Mater*. **2003**, *15*, 3930.

(14) Terazzi, E.; Bénech, J.-M.; Rivera, J.-P.; Bernardinelli, G.; Donnio, B.; Guillon, D.; Piguet, C. *Dalton Trans*. **2003**, 769.

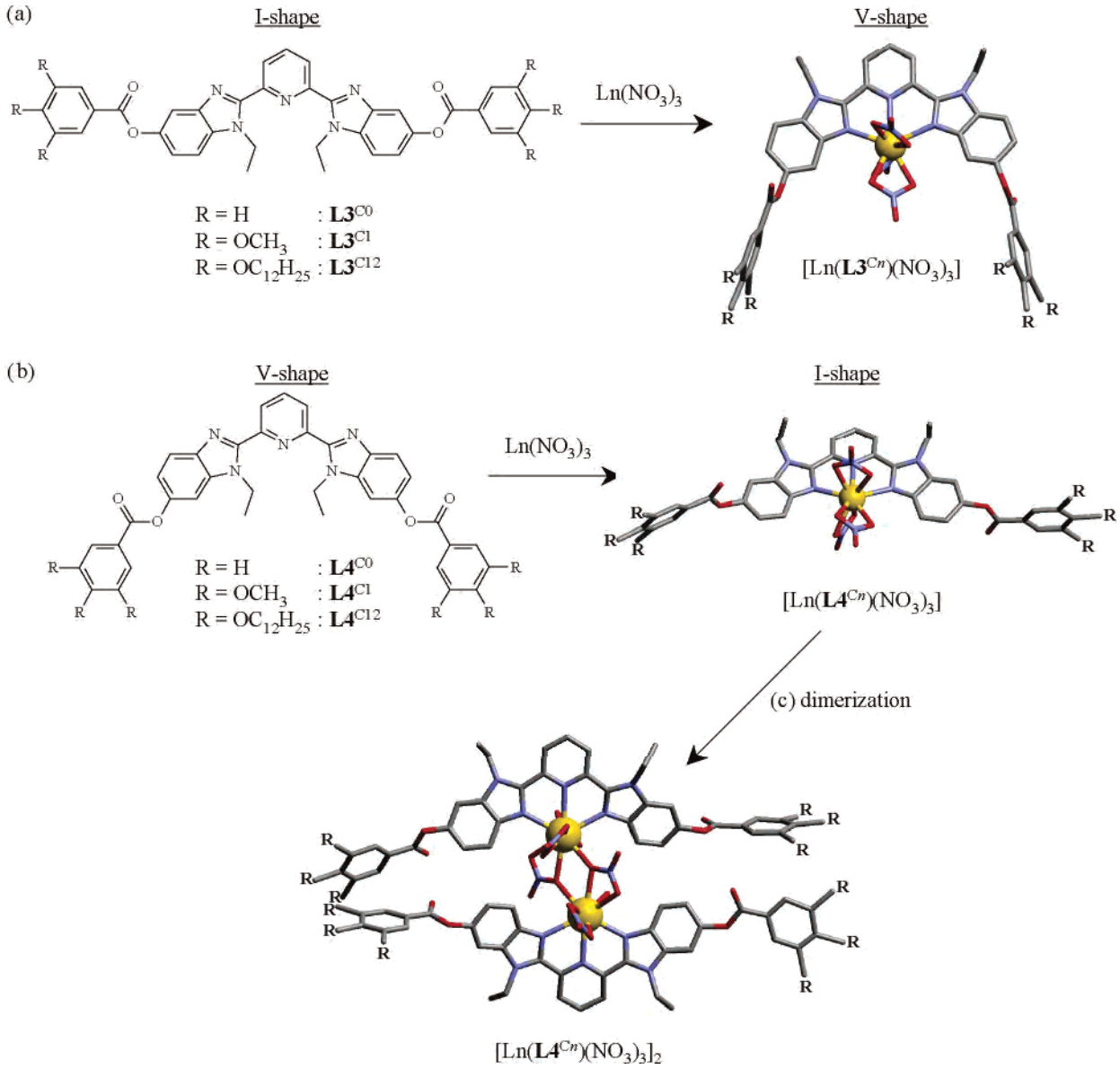

Figure 1. Formation of (a) monometallic V-shaped [Ln(**L3**^{Cn})$(NO_3)_3$] complexes, (b) monometallic I-shaped [Ln(**L4**^{Cn})$(NO_3)_3$] complexes, and c) rodlike dimers of [Ln(**L4**^{Cn})$(NO_3)_3]_2$. The molecular structures of the rigid cores of the complexes correspond to those found in the solid state by X-ray diffraction studies for (a) [Yb(**L3**^{C0})$(NO_3)_3$], (b) [Lu(**L4**^{C0})$(NO_3)_3$], and (c) [Eu(**L4**^{C0})$(NO_3)_3]_2$.[15]

small Ln(III) atoms, the compact packing of the monometallic hemidisklike [Ln(**L*i***^{C12})$(NO_3)_3$] complexes produces hexagonal columnar organization in the mesophases, while the loosening of intracolumnar interactions for midrange Ln(III) transforms columnar organization into body-centered cubic organization.[15] Finally, the formation of rodlike nitrato-bridged dimers, [Ln(**L*i***^{C12})$(NO_3)_3]_2$, with large Ln(III) atoms reduces the curvature of the molecular interface to such an extent that layered organization (lamello-columnar) results (Figure 1c).[15]

This minute manipulation of the molecular structures of the complexes suggests that X-bridged [Ln(**L*i***^{C12})$(X)_3]_2$ dimers could be interesting candidates for forcing the lanthanide-containing liquid-crystalline phases to adopt fluid smectic or fast-reorienting nematic organizations, a prerequisite for the design of new materials for liquid-crystal displays (LCD)[16] with improved magnetic[8,17] and optical (i.e., luminescent)[18] properties. The previous isolation of the H-shape bimetallic dimers [Lu(**L5**)$(CF_3CO_2)_3]_2$[19] and [Lu(**L6**)$(CF_3CO_2)_3(H_2O)]_2$,[20] in which the two Ln(III) cations are bridged by trifluoroacetate anions (Figure 2), combined

(15) Terazzi, E.; Torelli, S.; Bernardinelli, G.; Rivera, J.-P.; Bénech, J.-M.; Bourgogne, C.; Donnio, B.; Guillon, D.; Imbert, D.; Bünzli, J.-C. G.; Pinto, A.; Jeannerat, D.; Piguet, C. *J. Am. Chem. Soc.* **2005**, *127*, 888.

(16) Kirsch, P.; Bremer, M. *Angew. Chem., Int. Ed.* **2000**, *39*, 4216.

(17) Binnemans, K.; van Deun, R.; Görller-Walrand, C.; Haase, W.; Bruce, D. W.; Malykhina, L.; Galyametdinov, Y. G. *Mater. Sci. Eng. C* **2001**, *C18*, 247.

(18) (a) Binnemans, K.; Moors, D. *J. Mater. Chem.* **2002**, *12*, 3374. (b) Van Deun, R.; De Fré, B.; Moors, D.; Binnemans, K. *J. Mater. Chem.* **2003**, *13*, 1520. (c) Driesen, K.; Binnemans, K. *Liq. Cryst.* **2004**, *31*, 601.

(19) Nozary, H.; Piguet, C.; Rivera, J.-P.; Tissot, P.; Bernardinelli, G.; Vulliermet, N.; Weber, J.; Bünzli, J.-C. G. *Inorg. Chem.* **2000**, *39*, 5286.

(20) Nozary, H.; Piguet, C.; Rivera, J.-P.; Tissot, P.; Morgantini, P.-Y.; Weber, J.; Bernardinelli, G.; Bünzli, J.-C. G.; Deschenaux, R.; Donnio, B.; Guillon, D. *Chem. Mater.* **2002**, *14*, 1075.

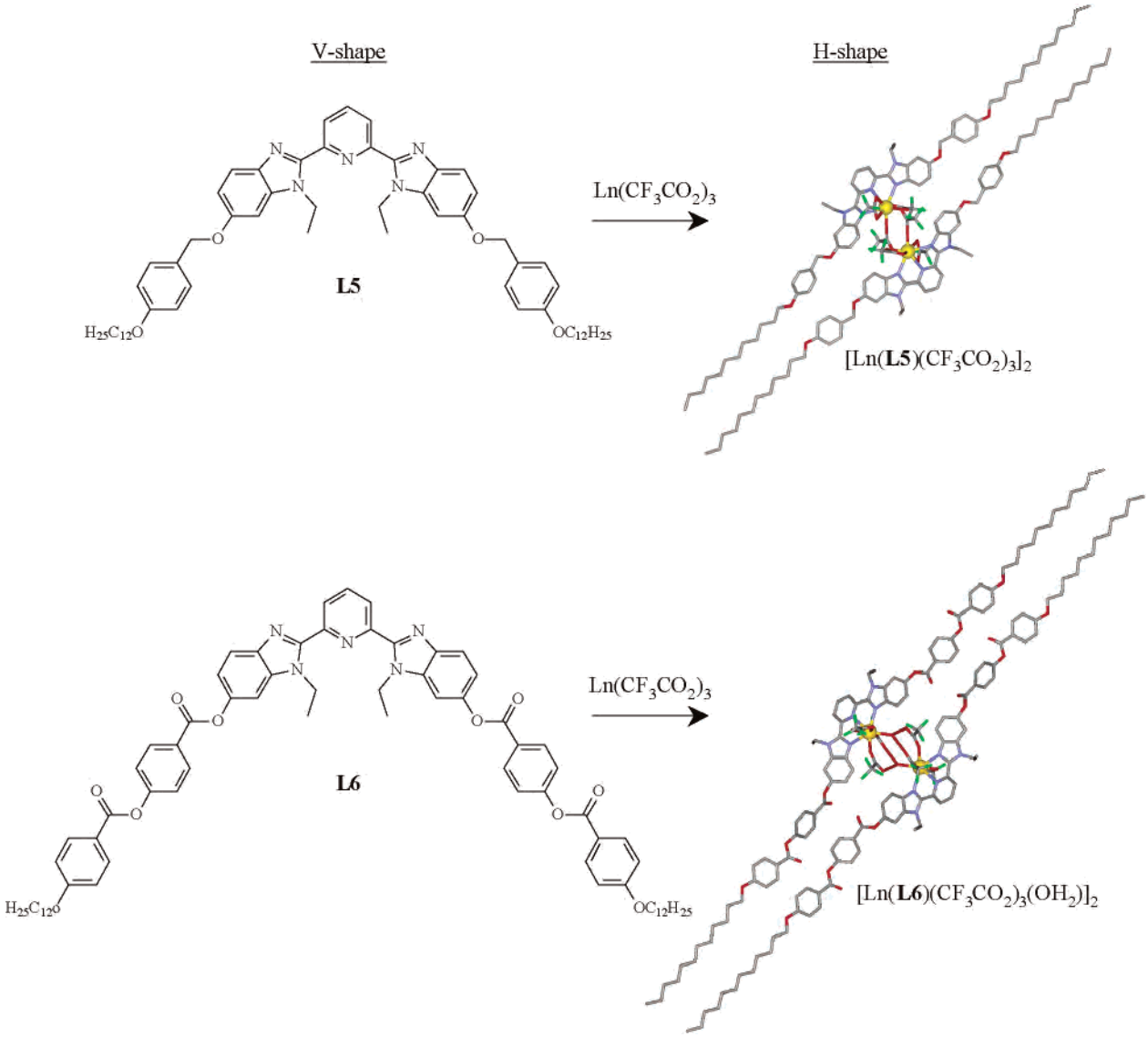

Figure 2. Formation of bimetallic H-shaped dimers bridged by trifluoroacetate anions. The molecular structures of the complexes correspond to those found in the solid state by X-ray diffraction studies for [Lu(**L5**)$(CF_3CO_2)_3]_2$[19] and [Lu(**L6**)$(CF_3CO_2)_3(OH_2)]_2$.[20]

with the well-established trend of substituted acetate anions $CR_3CO_2^-$ acting as a bridging ligand with Ln(III),[21] encourage us to investigate the related complexes formed between **L*i***^{C12} (i = 3, 4) and [Ln$(CF_3CO_2)_3$]. In this contribution, we report on the solid-state and solution structures of the polycatenar [Lu(**L*i***^{C12})$(CF_3CO_2)_3]_n$ (i = 3, 4; n = 1, 2) complexes, together with their thermodynamic stabilities and mesomorphic properties.

Results and Discussion

Preparation and Characterization of the [Ln(L*i*^{C12})-$(CF_3CO_2)_3$] (i = 3, 4; Ln = Pr, Sm, Gd, Ho, Yb, Lu, Y) Complexes in the Solid State. The [Lu(**L*i***^{C12})$(CF_3CO_2)_3$] (i = 3, 4) complexes are obtained by the stoichiometric mixing of **L*i***^{C12} (1 equiv)[15] with Ln$(CF_3CO_2)_3 \cdot x H_2O$ (x = 1−3) in acetonitrile/dichloromethane (1:1). Slow recrystallization from pure dichloromethane provides 80−95% of microcrystalline powders, whose elemental analyses (Table S1, Supporting Information) correspond to those of [Ln(**L3**^{C12})-$(CF_3CO_2)_3$] (Ln = Pr, **1**; Ln = Sm, **2**; Ln = Gd, **3**; Ln = Ho, **4**; Ln = Yb, **5**; Ln = Lu, **6**; Ln = Y, **7**) and [Ln(**L4**^{C12})$(CF_3$-$CO_2)_3] \cdot n H_2O$ (Ln = Pr, n = 2.5, **8**; Ln = Sm, n = 0, **9**; Ln = Gd, n = 0, **10**; Ln = Ho, n = 0, **11**; Ln = Yb, n = 0, **12**; Ln = Lu, n = 0.5, **13**; Ln = Y, n = 0, **14**). For the anhydrous complexes **1**−**7**, **9**−**12**, and **14**, thermogravimetric analyses (TGA) confirm the absence of weight loss prior to decomposition occurring around 240−270 °C (Table 8). For the hydrated complexes **8** and **13**, TGA shows that 2.2 and 0.8 water molecules are respectively lost prior to decomposition (Table 8), in good agreement with the elemental analyses (Table S1, Supporting Information). Attempts to obtain monocrystals with complexes **1**−**14** only failed, but the analogous less lipophilic model complexes, [Lu(**L4**^{C0})$(CF_3$-

(21) (a) Junk, P. C.; Kepert, C. J.; Min, L. W.; Skelton, B. W.; White, A. H. *Aust. J. Chem.* **1999**, *52*, 437. (b) Junk, P. C.; Kepert, C. J.; Min, L. W.; Skelton, B. W.; White, A. H. *Aust. J. Chem.* **1999**, *52*, 459. (c) Kepert, C. J.; Min, L. W.; Semenova, L. I.; Skelton, B. W.; White, A. H. *Aust. J. Chem.* **1999**, *52*, 481. (d) Zhang, J.; Morlens, S.; Hubert-Pfalzgraf, L. G.; Luneau, D. *Eur. J. Inorg. Chem.* **2005**, 3928.

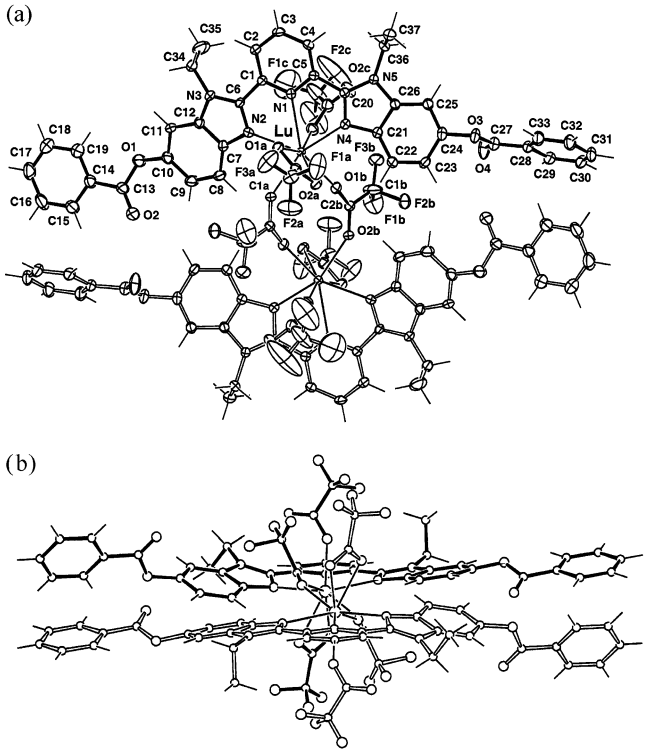

Figure 3. Perspective views of [Lu(**L4**^{C0})$(CF_3CO_2)_3]_2$ in the crystal of **15**; a) almost perpendicular to the aromatic planes of the tridentate binding unit with numbering scheme for the asymmetric unit and b) along the Lu···Lu direction. Ellipsoids are represented at the 40% probability level.

$CO_2)_3]$, provide X-ray quality crystals upon recrystallization from dry propionitrile ([Lu(**L4**^{C0})$(CF_3CO_2)_3]_2$, **15**) or from a wet nitromethane solution upon slow diffusion of diethyl ether ([Lu(**L4**^{C0})$(CF_3CO_2)_3(H_2O)]\cdot 0.3H_2O$, **16**). Despite considerable efforts dedicated to the preparation of related monocrystals with [Ln(**L3**^{Cn})$(CF_3CO_2)_3]$, we only succeeded in isolating crystals of sufficient quality for [La(**L3**^{C4})$(CF_3CO_2)_3]_2$ (**17**).

Crystal and Molecular Structures of the Complexes [Lu(L4^{C0})$(CF_3CO_2)_3]_2$ (15), [Lu(L4^{C0})$(CF_3CO_2)_3(H_2O)]\cdot 0.3H_2O$ (16), and [La(L3^{C4})$(CF_3CO_2)_3]_2$ (17). The crystal structure of **15** is composed of centrosymmetric dimers [Lu(**L4**^{C0})$(CF_3CO_2)_3]_2$, in which the metals are separated by 5.7170(5) Å, connected by two bridging trifluoroacetate anions (Figure 3 and Table 1). Each Lu(III) is eight-coordinated by the three heterocyclic nitrogen atoms of the I-shaped tridentate aromatic ligand **L4**^{C0} and by five oxygen atoms of two bridging monodentate $CF_3CO_2^-$ units, one terminal monodentate $CF_3CO_2^-$ and one terminal bidentate $CF_3CO_2^-$, the two terminal anions being located on opposite sides of the meridional plane defined by N1, N2, N4 (Figure 3b). Lu(III) lies only slightly out of this plane (deviation of 0.063(5) Å toward the bidentate trifluoroacetate a, Figure 3b), and it displays Lu−N distances (2.398−2.498 Å, average 2.45(5) Å) slightly shorter than those found in [Lu(**L5**)$(CF_3CO_2)_3]_2$ (2.460−2.544 Å, average 2.50(4) Å).[19] However, Lu(III) is nine-coordinate in the latter complex, but it is only eight-coordinated in [Lu(**L4**^{C0})$(CF_3CO_2)_3]_2$. The application of the standard correction accompanying the increase of ionic radius[22] on going from $R_{Lu}^{CN=8} = 0.977$ Å to $R_{Lu}^{CN=9} = 1.032$ Å leads to an average value of Lu−N(corr) = 2.51(5) Å for [Lu(**L4**^{C0})$(CF_3CO_2)_3]_2$ (Table 2, entry 3), which perfectly fits the Lu−N bond length found in [Lu(**L5**^{C0})$(CF_3CO_2)_3]_2$. We conclude that, except for the replacement of one terminal monodentate with a bidentate trifluoroacetate when going from [Lu(**L4**^{C0})$(CF_3CO_2)_3]_2$ to [Lu(**L5**)$(CF_3CO_2)_3]_2$,[19] both structures are similar (Figure S1, Supporting Information).

Table 1. Selected Bond Distances (Å) and Angles (deg) for [Lu(**L4**^{C0})$(CF_3CO_2)_3]_2$ (**15**)[a]

Bond Distances			
Lu···Lu′	5.7170(5)	Lu−O2b′	2.271(2)
Lu−O1a	2.356(4)	Lu−N2	2.460(3)
Lu−O1b	2.264(3)	Lu−O1c	2.206(3)
Lu−N1	2.498(3)	Lu−N4	2.398(3)
Lu−O2a	2.481(3)		
N−Lu−N Bite Angles			
N1−Lu−N2	65.0(1)	N2−Lu−N4	131.2(1)
N1−Lu−N4	66.2(1)		
N−Lu−O Angles			
N1−Lu−O1a	73.2(1)	N4−Lu−O1a	85.1(1)
N1−Lu−O1c	76.1(1)	N4−Lu−O1c	88.9(1)
N2−Lu−O2a	130.4(1)	N1−Lu−O1b	144.5(1)
N2−Lu−O1c	78.0(1)	N2−Lu−O1a	83.0(1)
N4−Lu−O1b	87.9(1)	N2−Lu−O2b′	76.1(1)
N1−Lu−O2a	116.0(1)	N4−Lu−O2a	74.5(1)
N1−Lu−O2b′	135.88(9)	N4−Lu−O2b′	148.1(1)
N2−Lu−O1b	133.7(1)		
O−Lu−O Angles			
O1a−Lu−O2a	54.4(1)	O1b−Lu−O1c	79.6(1)
O1a−Lu−O2b′	82.5(1)	O1a−Lu−O1c	148.6(1)
O2a−Lu−O2b′	74.4(1)	O2a−Lu−O1c	151.4(1)
O1c−Lu−O2b′	116.2(1)	O1b−Lu−O2b′	78.5(1)
O1a−Lu−O1b	130.8(1)		
O2a−Lu−O1b	76.8(1)		

[a] The atoms with a prime correspond to those obtained by the symmetry operation $1 - x$, $1 - y$, $1 - z$.

Interestingly, the Lu−N distances in trifluoroacetate complexes are significantly longer than those reported for the analogous nitrato complexes, [Lu(**L4**^{C0})$(NO_3)_3]$[15] and [Lu(**L5**)$(NO_3)_3]$[19] (Table 2), but the ionic radii of Lu(III) calculated according to Shannon's definition[22] with r(N) = 1.46 Å, $r(O_{trifluoroacetate}) = 1.35$ Å, and $r(O_{nitrate}) = 1.31$ Å[23] for trifluoroacetate dimers and for nitrato complexes, respectively, match those expected for eight-coordinate Lu(III) (0.977 Å) and nine-coordinate Lu(III) (1.032 Å, Table 2).[22] We deduce that no special constraints occur within the lanthanide coordination spheres, but a detailed geometrical analysis shows that, after adaptation of all Lu−N bond distances for CN = 9, the Ln−N(pyridine) and the Lu−N(benzimidazole) bonds are systematically longer by ∼0.1 Å in the trifluoroacetate dimers (Table 2). The origin of this loosening of the Lu−N bonds in [Lu(**L*i***)$(CF_3CO_2)_3]_2$ (i = 4, 5) can be thus assigned to the replacement of peripheral nitrate with trifluoroacetate anions. This effect can be reasonably attributed to the larger negative charge borne by the oxygen atoms of the trifluoroacetates, which reduces the global positive charge of the metal upon complexation and, consequently, its affinity for the additional neutral tridentate ligand.

(22) Shannon, R. D. *Acta Cryst.* **1976**, *A32*, 751.
(23) Bünzli, J.-C. G.; Klein, B.; Chapuis, G.; Schenk, K. J. *Inorg. Chem.* **1982**, *21*, 808.

Table 2. Geometrical Analysis of Lu−N Bond Distances and Lu(III) Ionic Radii in [Lu(**L4**^{C0})$(CF_3CO_2)_3]_2$ (**15**), [Lu(**L4**^{C0})$(CF_3CO_2)_3(H_2O)]$ (**16**), [Lu(**L5**)$(CF_3CO_2)_3]_2$, [Lu(**L4**^{C0})$(NO_3)_3]$, and [Lu(**L5**)$(NO_3)_3]$

complexes	CN[a]	R_{Lu} (Å)	Ln−N(py) (Å)	Ln−N(bzim) (Å)[b]	av Ln−N (Å)[b]	ref
[Lu(**L4**^{C0})$(CF_3CO_2)_3]_2$	8	0.976	2.498	2.42(4)	2.45(5)	this work
[Lu(**L4**^{C0})$(CF_3CO_2)_3(H_2O)]$	8	0.962	2.499	2.43(3)	2.45(5)	this work
[Lu(**L4**^{C0})$(CF_3CO_2)_3]_2$	9[c]		2.553	2.48(4)	2.51(5)	this work
[Lu(**L4**^{C0})$(CF_3CO_2)_3(H_2O)]$	9[c]		2.554	2.48(3)	2.51(5)	this work
[Lu(**L5**)$(CF_3CO_2)_3]_2$	9	1.031	2.544	2.47(1)	2.50(4)	19
[Lu(**L4**^{C0})$(NO_3)_3]$	9	1.032	2.466	2.39(2)	2.42(4)	15
[Lu(**L5**)$(NO_3)_3]$	9	1.028	2.445	2.383(8)	2.40(4)	19

[a] CN = coordination number. [b] Standard deviations of the average values are given in parentheses. [c] Adapted for nine-coordinate Lu(III) according to $\Delta R = R_{Lu}^{CN=9} - R_{Lu}^{CN=8} = 1.032-0.977 = 0.055$ Å.[22]

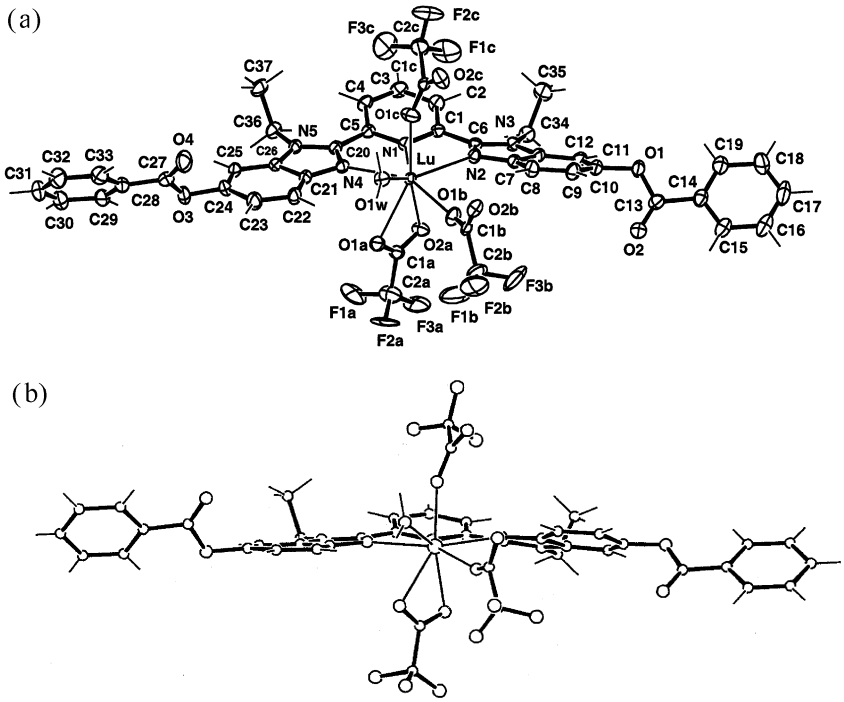

Figure 4. Perspective views of [Lu(**L4**^{C0})$(CF_3CO_2)_3(H_2O)]$ in the crystal of **16**: (a) almost perpendicular to the aromatic planes of the tridentate binding unit with numbering scheme and (b) along the Lu−N1 direction. Ellipsoids are represented at the 40% probability level.

Upon crystallization from wet nitromethane, one water molecule replaces the bridging trifluoroacetate anion around Lu(III), and the monometallic eight-coordinate complex [Lu(**L4**^{C0})$(CF_3CO_2)_3(H_2O)]$ is found in the crystal structure of **16** (Figure 4 and Table 3). Lu(III) still lies slightly out of the N1, N2, N4 plane defined by the coordinated nitrogen atoms of the I-shaped tridentate aromatic ligand (deviation of 0.250(4) Å toward the bidentate trifluoroacetate a, Figure 4b), and the Ln−N bond distances strictly parallel those obtained for the dimer [Lu(**L4**^{C0})$(CF_3CO_2)_3]_2$ (**15**, Table 2). The metallic coordination spheres in **15** and **16** are roughly superimposable (Figure S2, Supporting Information). The only noticeable difference concerns the metallic ionic radius $R_{Lu}^{CN=8} = 0.962$ Å in **16**, which is slightly smaller than that expected for eight-coordinate Lu(III) centers (0.977 Å),[22] a value indeed found in **15** (Table 2). This minor change can be assigned to the replacement of two bridging Ln−O(trifluoroacetate) bonds in the dimer (average distance = 2.268(5) Å) with one Lu−O(water) bond (Lu−O1w = 2.276(3) Å) and one monodentate Lu−O(trifluoroacetate) bond (Lu−O1b = 2.201(3) Å). Detailed interplanar angles characterizing the minor torsions of the aromatic rings within each tridentate binding unit in **15** and **16** (7−28°) can be found in Tables S2 and S3, while the specific weak intermolecular π-stacking occurring in the crystal structures of **15** and **16** is illustrated in Figures S3 and S4 (Supporting Information).

Although the scattered intensities collected for [La(**L3**^{C4})$(CF_3CO_2)_3]_2$ (**17**) are rather weak because of the large disorder affecting the butyloxy chains and some trifluoroacetate anions (see Experimental Section), they correspond to the best results obtained with these types of complexes, and the refinement of the central rigid core is satisfactory. The crystal structure of **17** is composed of centrosymmetric dimers of [La(**L3**^{C4})$(CF_3CO_2)_3]_2$, in which the metals are separated by 4.7955(8) Å (Figure 5 and Table 4). Since we observe that trifluoroacetate c is distributed over two positions, one corresponding to a monodentate binding mode (40%) and the second displaying a bidentate binding mode (60%, Figure S5, Supporting Information), we calculate that each La(III) atom possesses an average coordination number of 8.6 with three nitrogen atoms of the tridentate ligand, four

Table 3. Selected Bond Distances (Å) and Angles (deg) for $[Lu(\mathbf{L4}^{C0})(CF_3CO_2)_3(H_2O)]\cdot 0.3H_2O$ (**16**)

	Bond Distances		
Lu−O1a	2.435(3)	Lu−O1w	2.276(3)
Lu−O1b	2.201(3)	Lu−N2	2.446(3)
Lu−N1	2.499(3)	Lu−O1c	2.190(4)
Lu−O2a	2.370(4)	Lu−N4	2.407(3)
	N−Lu−N Bite Angles		
N1−Lu−N2	66.11(9)	N2−Lu−N4	131.9(1)
N1−Lu−N4	66.4(1)		
	N−Lu−O Angles		
N1−Lu−O1a	111.66(9)	N4−Lu−O1a	73.9(1)
N1−Lu−O1c	77.0(1)	N4−Lu−O1c	85.0(1)
N2−Lu−O2a	81.0(1)	N1−Lu−O1b	138.8(1)
N2−Lu−O1c	77.5(1)	N2−Lu−O1a	132.1(1)
N4−Lu−O1b	148.74(9)	N2−Lu−O1w	134.38(9)
N1−Lu−O2a	74.6(1)	N4−Lu−O2a	93.7(1)
N1−Lu−O1w	140.8(1)	N4−Lu−O1w	82.4(1)
N2−Lu−O1b	77.9(1)		
	O−Lu−O Angles		
O1a−Lu−O2a	54.7(1)	O2a−Lu−O1b	80.8(1)
O1a−Lu−O1w	79.6(1)	O1b−Lu−O1c	115.0(1)
O2a−Lu−O1w	132.99(9)	O1a−Lu−O1c	150.3(1)
O1c−Lu−O1w	77.2(1)	O2a−Lu−O1c	149.5(1)
O1a−Lu−O1b	78.0(1)	O1b−Lu−O1w	79.4(1)

oxygen atoms of four bridging trifluoroacetate anions, and 1.6 oxygen of the disordered trifluoroacetate c. The V-shaped arrangement of the meridionally tricoordinated ligand $\mathbf{L3}^{C4}$ in **17** precludes the head-to-head approach of two monomeric $[La(\mathbf{L3}^{C4})(CF_3CO_2)_3]$ units, as found for the related I-shaped ligand $\mathbf{L4}^{C0}$ in $[Lu(\mathbf{L4}^{C0})(CF_3CO_2)_3]_2$ (**16**, Figure 3) or in $[Lu(\mathbf{L5})(CF_3CO_2)_3]_2$ (Figure 2).[19] Consequently, the two aromatic tridentate binding units in $[La(\mathbf{L3}^{C4})(CF_3CO_2)_3]_2$ adopt a parallel face-to-face arrangement, which forces the lanthanum atoms to occupy positions significantly outside the chelating N1, N2, N4 plane (deviation of 1.03(1) Å toward the second metal ion, Figure 5b), thus offering sufficient access for the formation of four intermetallic trifluoroacetate bridges.

The La−N and La−O bond distances are standard (Table 4), as exemplified by the ionic radii $R_{La}^{CN=8} = 1.14$ Å (expected 1.160 Å)[22] and $R_{La}^{CN=9} = 1.20$ Å (expected 1.216 Å)[22] calculated for $[La(\mathbf{L3}^{C4})(CF_3CO_2)_3]_2$ for both isomers containing either a monodentate (CN = 8) or a bidentate (CN = 9) trifluoroacetate c, respectively. If we apply the correction $R_{La}^{CN=8} - R_{Lu}^{CN=8} = 1.160 - 0.977 = 0.183$ Å[22] to the La−N bonds found in $[La(\mathbf{L3}^{C4})(CF_3CO_2)_3]_2$, we predict average bond distances of Lu−N(pyridine) = 2.525 Å and Lu−N(benzimidazole) = 2.465 Å, which compare well with related Lu−N bonds observed in $[Lu(\mathbf{L4}^{C0})(CF_3CO_2)_3]_2$ (**15**) and $[Lu(\mathbf{L4}^{C0})(CF_3CO_2)_3(H_2O)]$ (**16**) (Table 2). This observation confirms that the loosening of the Lu−N interaction is asssociated with the concomitant binding of trifluoroacetate anions and not with the specific anisometries of the tridentate ligands.

Stabilities and Structures of the $[Ln(Li^{C12})(CF_3CO_2)_3]$ Complexes in Solution. To investigate the effect of the ionic radius of Ln(III) on the solution structures of the complexes $[Ln(\mathbf{L}i^{C12})(CF_3CO_2)_3]$ (i = 3, 4), we have investigated the diamagnetic complexes with Ln = La (the largest lanthanide), Ln = Y (a midrange cation similar in size to Ho),[22] and Ln = Lu (the smallest lanthanide). The ^{1}H NMR spectrum of

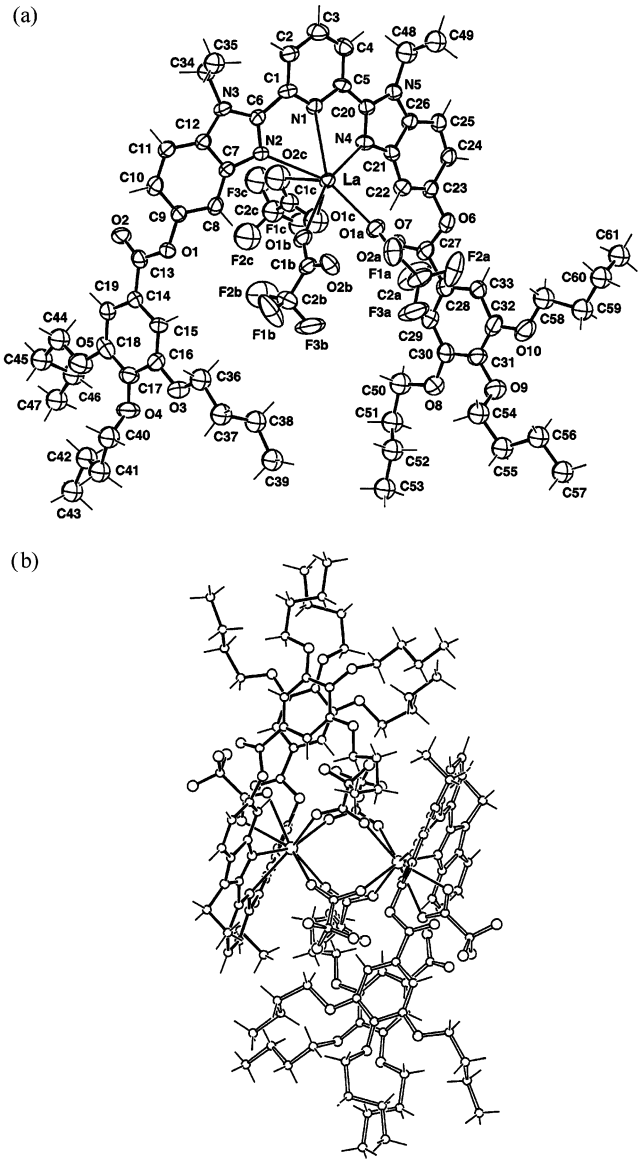

Figure 5. Perspective views of the major nine-coordinate isomer $[La(\mathbf{L3}^{C4})(CF_3CO_2)_3]_2$ in the crystal of **17**: (a) representation of the asymmetric unit with numbering scheme and (b) view perpendicular to the La···La direction. Ellipsoids are represented at the 30% probability level, and the C atoms of the butyl chains are shown with a fixed U_{iso} of 0.1 Å^2 for clarity.

$[Lu(\mathbf{L3}^{C12})(CF_3CO_2)_3]$ (**6**) in CD_2Cl_2 (10^{-2} mol dm^{-3}, 298 K) shows twelve aromatic signals assigned to two independent sets of protons Hi (i = 1−6, numbering in Figure 6), together with two quartets originating from two sets of enantiotopic methylene protons, H8 and H8′ (Figure 6a). This pattern corresponds to the coexistence of two C_{2v}-symmetrical ligands, $\mathbf{L3}^{C12}$, in different environments in an 85:15 ratio and under a slow exchange regime on the NMR time scale. Comparison with the ^{1}H NMR spectrum of the free ligand $\mathbf{L3}^{C12}$ shows an exact match with the spectrum of the minor component (15%, Table 5), while the large downfield shift ($\Delta\delta$ = 0.36 ppm) of the proton H1 in the major species is diagnostic for the complexation of the pyridine ring to Lu(III).[15,24] Variable-temperature measure-

(24) Lavallee, D. K.; Baughman, M. D.; Phillips, M. P. *J. Am. Chem. Soc.* **1977**, *99*, 718.

Table 4. Selected Bond Distances (Å) and Angles (deg) for $[La(\mathbf{L3}^{C4})(CF_3CO_2)_3]_2$ (**17**)[a]

Bond Distances			
La···La″	4.7955(8)	La−O2b	2.504(6)
La−O1a	2.495(8)	La−O2c	2.70(1)
La−O1b	2.475(9)	La−N2	2.642(7)
La−O1c	2.66(1)	La−O1c′	2.27(1)
La−N1	2.708(9)	La−N4	2.654(8)
La−O2a	2.474(7)		
N−La−N Bite Angles			
N1−La−N2	60.9(2)	N2−La−N4	114.8(3)
N1−La−N4	60.1(2)		
N−La−O Angles			
N1−La−O1a	140.4(2)	N2−La−O1c	104.0(3)
N1−La−O1c	113.6(4)	N4−La−O2a	126.5(3)
N2−La−O1a	157.6(3)	N4−La−O2b	68.8(2)
N2−La−O2b	122.0(2)	N1−La−O1b	143.4(2)
N4−La−O1a	82.3(3)	N1−La−O2c	76.1(4)
N4−La−O1c	76.9(4)	N2−La−O1b	83.6(3)
N1−La−O2a	83.5(3)	N2−La−O2c	62.0(4)
N1−La−O2b	78.6(2)	N4−La−O1b	154.7(2)
N2−La−O2a	69.2(2)	N4−La−O2c	79.4(4)
O−La−O Angles			
O1a−La−O2a	113.3(3)	O1c−La−O2c	46.4(5)
O1a−La−O2b	76.5(2)	O1b−La−O2c	96.1(4)
O2a−La−O2b	66.5(2)	O1a−La−O1c	64.3(4)
O1c−La−O2b	130.6(3)	O2a−La−O1c	156.6(4)
O1a−La−O2c	110.6(4)	O1b−La−O2b	117.4(3)
O1a−La−O1b	76.0(3)	O2c−La−O2b	146.4(4)
O2a−La−O1b	75.0(3)	O2a−La−O2c	131.1(4)
O1b−La−O1c	82.0(4)		

[a] The atoms with a prime correspond to those of the minor isomer, in which the trifluoroacateate c is monodentate (Figure S5, Supporting Information). The atoms with a double prime correspond to those obtained by the symmetry operation $-x, -y, 1 - z$.

ments indicate that the quantity of free $\mathbf{L3}^{C12}$ increases with increasing temperature from 0% at 273 K to 20(2)% at 313 K (Figure 6b and Table S5, Supporting Information).

Assuming that (i) the Einstein−Smoluchowski−Stokes auto-diffusion theory holds for our lipophilic complexes in CD_2Cl_2 and that (ii) both the free ligand and its complexes in solution can be roughly modeled with spheres possessing specific hydrodynamic radius r_h, the auto-diffusion coefficients for a component m, D_m, at a fixed temperature in CD_2Cl_2 is proportional to $(\bar{\nu}_m\, MM_m)^{-1/3}$, where MM_m stands for the molecular weight of the molecule and $\bar{\nu}_m$ for its specific partial volume.[25] The ratio of the auto-diffusion coefficients of the two species (complex and free ligand $\mathbf{L3}^{C12}$) in CD_2Cl_2 is related to their molecular weights according to eq 1. Diffusional NMR is thus an efficient tool for deducing the molecular mass of the unknown complex $MM_{complex}$ existing in equilibrium with the free ligand.[26]

$$\frac{D_{Ligand}}{D_{Complex}} = \sqrt[3]{\frac{\bar{\nu}_{Complex} MM_{Complex}}{\bar{\nu}_{Ligand} MM_{Ligand}}} \qquad (1)$$

NMR-DOSY experiments for $[Lu(\mathbf{L3}^{C12})(CF_3CO_2)_3]$ (**6**) give $D_{Ligand}/D_{Complex} = 1.04(4)$ (CD_2Cl_2, 10^{-2} mol dm^{-3}, 293 K, Table 6). Considering the density found in the crystal structures of $\mathbf{L3}^{C4}$ ($d = 1.186$ g cm^{-3})[14] and $[Lu(\mathbf{L6})(CF_3CO_2)_3(OH_2)]_2$ ($d = 1.464$ g cm^{-3})[20] as reasonable approximations for respectively $(\bar{\nu}_{Ligand})^{-1}$ and $(\bar{\nu}_{Complex})^{-1}$ in solution, we calculate with eq 1 that $MM_{Complex}/MM_{Ligand} = 1.3(2)$. This translates into $MM_{Complex} = 2330(250)$ g mole^{-1}, which matches the value of MM = 2227.6 g mole^{-1} calculated for the monomer $[Lu(\mathbf{L3}^{C12})(CF_3CO_2)_3]$ but cannot account for the value of MM = 4455.2 g mole^{-1} predicted for the bimetallic bridged dimer $[Lu(\mathbf{L3}^{C12})(CF_3CO_2)_3]_2$. We conclude that $[Lu(\mathbf{L3}^{C12})(CF_3CO_2)_3]$ exists as a monomer in CD_2Cl_2, which is partially dissociated according to eq 2 ($i = 3$, Ln = Lu).

$$\mathbf{L}i^{C12} + Ln(CF_3CO_2)_3 \rightleftharpoons [Lu(\mathbf{L}i^{C12})(CF_3CO_2)_3] \qquad \beta_{LnLi}^{CF3CO2} \qquad (2)$$

Closely related behaviors compatible with eq 2 are obtained for $[Y(\mathbf{L3}^{C12})(CF_3CO_2)_3]$ (**8**) and $[Ln(\mathbf{L4}^{C12})(CF_3CO_2)_3]$ (Ln = Lu, **13**; Ln = Y, **14**; Tables 5, 6, and S6−S8), while the occurrence of intermediate ligand-exchange processes on the NMR time scale for $[La(\mathbf{L}i^{C12})(CF_3CO_2)_3]$ ($i = 3, 4$) broadens the ^{1}H NMR signals to such an extent that a detailed analysis of thermodynamic equilibrium is precluded. The partial dissociation of the neutral tridentate ligand $\mathbf{L}i^{C12}$ seen in the trifluoroacetate complexes at millimolar concentration in noncoordinating solvent, strongly contrasts with the quantitative formation of related nitrato complexes $[Ln(\mathbf{L}i^{C12})(NO_3)_3]$ (Ln = Lu, Y) under the same conditions.[15] We thus conclude that the loosening of the Ln−N bonds exemplified in the solid state upon the replacement of coordinated NO_3^- with $CF_3CO_2^-$ is maintained in solution. The quantitative treatment of the ratios of bound and free ligands observed for $[Ln(\mathbf{L}i^{C12})(CF_3CO_2)_3]$ at each temperature (Ln = Lu, Y, $i = 3, 4$, Tables S5−S8, Supporting Information) by using the van't Hoff equation (eq 3)[15] allows for a a rough estimation of $\log(\beta_{LnLi}^{CF3CO2})$, together with ΔH_{LnLi}^{CF3CO2} and ΔS_{LnLi}^{CF3CO2} in CD_2Cl_2 at 293 K (Table 7).

$$-R \ln(\beta_{LnLi}^{CF3CO2}) = \frac{\Delta H_{LnLi}^{CF3CO2}}{T} - \Delta S_{LnLi}^{CF3CO2} \qquad (3)$$

Interestingly, the value of $\log(\beta_{LnLi}^{CF3CO2})$ (3.1−4.2) estimated from the VT-NMR data for $[Ln(\mathbf{L}i^{C12})(CF_3CO_2)_3]$ (Table 7) is approximately 2 orders of magnitude smaller than the one ($\log(\beta_{LnLi}^{NO3}) = 5.3-6.1$) reported for $[Ln(\mathbf{L3}^{C12})(NO_3)_3]$ in acetonitrile/dichloromethane (1:1, Table 7).[15] To obtain comparable thermodynamic data, we perform complementary spectrophotometric titrations of $\mathbf{L3}^{C12}$ with $Ln(CF_3CO_2)\cdot xH_2O$ ($x = 1-3$) in CH_3CN/CH_2Cl_2 (1:1). We systematically observe a single smooth end point for the ratio, $\mathbf{L3}^{C12}/Ln = 1.0$, together with isosbestic points during the complete titration (Ln = La, Eu, Y, Lu, Figure 7). The experimental data can be satisfyingly fitted with nonlinear

(25) (a) Stilbs, P. *Prog. NMR Spectrosc.* **1986**, *19*, 1. (b) Waldeck, A. R.; Kuchel, P. W.; Lennon, A. J.; Chapman, B. E. *Prog. NMR Spectrosc.* **1997**, *30*, 39. (c) Pregosin, P. S.; Martinez-Viviente, E.; Anil Kumar, P. G. *Dalton Trans.* **2003**, 4007. (d) Pregosin, P. S.; Kumar, P. G. A.; Fernandez, I. *Chem. Rev.* **2005**, **105**, 2977.
(26) Greenwald, M.; Wessely, D.; Goldberg, I.; Cohen, Y. *New J. Chem.* **1999**, 337.

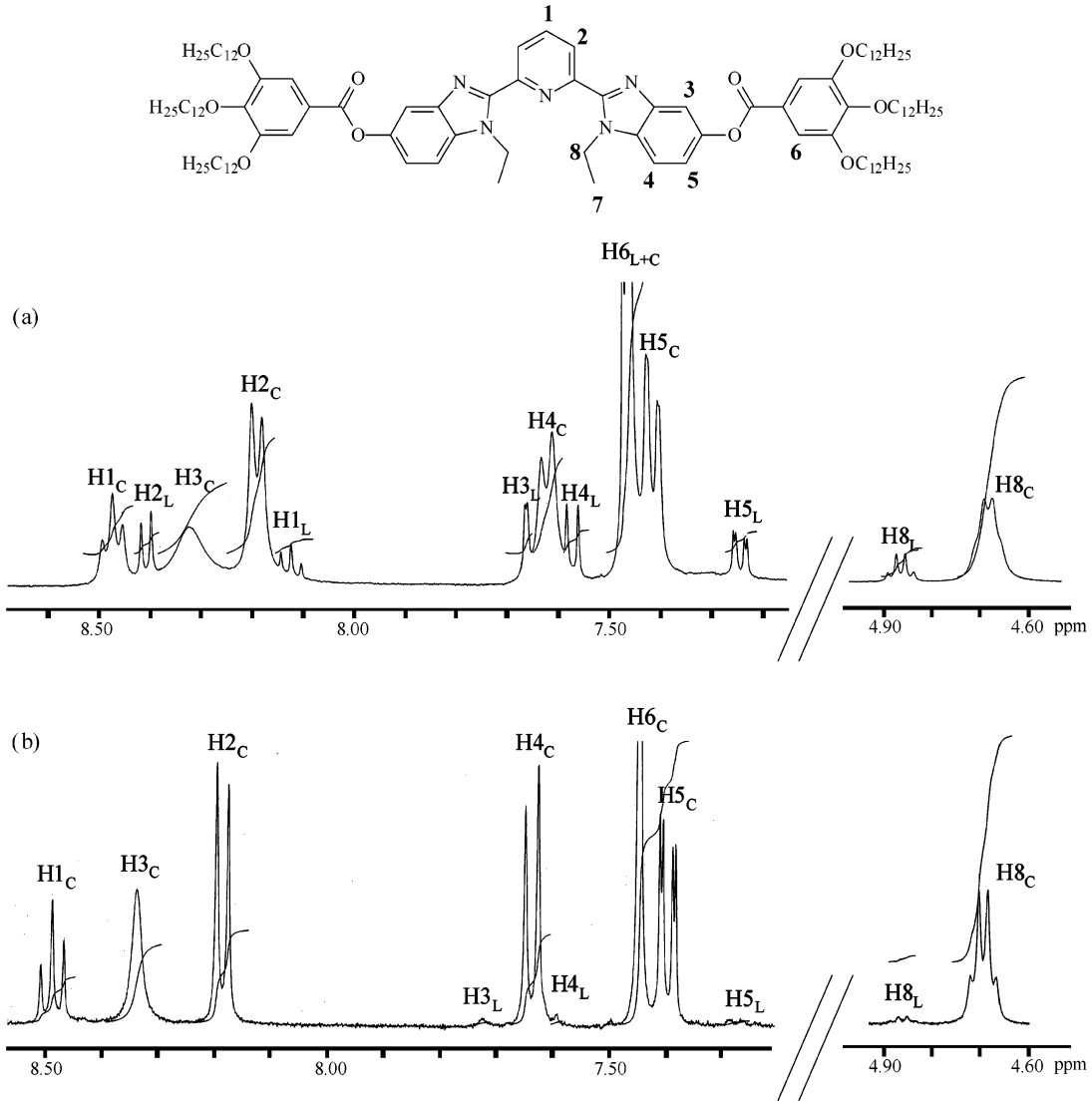

Figure 6. ^{1}H NMR spectra of [Lu(**L3**^{C12})$(CF_3CO_2)_3$] (**6**) with numbering scheme (10^{-2} mol dm^{-3}, CD_2Cl_2) at (a) 298 K (complex/ligand = 85:15) and (b) 283 K (complex/ligand = 98:2). The indexes L and C stand for ligand and complex, respectively.

Table 5. ^{1}H NMR Shifts (in ppm with Respect to TMS) for the Ligands **L*i***^{C12} and for the Complexes [Ln(**L*i***^{C12})$(CF_3CO_2)_3$] (i = 3, 4; Ln = Lu, Y, CD_2Cl_2; 298 K)[a]

	H1	H2	H3	H4	H5	H6	H7	H8
L3^{C12}	8.10	8.40	7.63	7.55	7.22	7.46	1.42	4.87
[Lu(**L3**^{C12})$(CF_3CO_2)_3$]	8.47	8.18	8.34	7.63	7.40	7.46	1.77	4.69
[Y(**L3**^{C12})$(CF_3CO_2)_3$]	8.44	8.12	8.24	7.60	7.39	7.42	1.77	4.66
L4^{C12}	8.10	8.39	7.39	7.85	7.17	7.46	1.38	4.84
[Lu(**L4**^{C12})$(CF_3CO_2)_3$]	8.47	8.17	7.52	8.51	7.34	7.45	1.76	4.67
[Y(**L4**^{C12})$(CF_3CO_2)_3$]	8.42	8.11	7.47	8.38	7.26	7.44	1.73	4.62

[a] Numbering of the protons H*i* in Figure 6.

least-squares techniques[27] to eq 2 to give $\log(\beta_{\mathrm{LnL}i}^{\mathrm{CF3CO2}}) = 4.4-4.5$ (Table 7), which confirms a decrease in stability of about 1−2 orders of magnitude when nitrate counteranions are replaced with trifluoroacetates.

We can safely conclude that, in poorly coordinating solvents, $Ln(CF_3CO_2)_3$ less efficiently interacts with the tridentate ligands **L*i***^{C12} than does $Ln(NO_3)_3$, thus leading to monometallic [Ln(**L*i***^{C12})$(CF_3CO_2)_3$] complexes, which are partially dissociated at millimolar concentrations. Moreover, we do not detect dimerization processes occurring in solution, which strongly contrasts with the solid-state structures of **15** and **17**. In this context, we suspect that the entropic cost of the dimerization process cannot be overcome by the minor enthalpic gain accompanying the transformation of two bidentate trifluoroacetates (2 [LnO_2C]) into two bridging trifluoroacetates ([Ln−O−C−O−Ln]) in solution. Finally, the enthalpic $\Delta H_{\mathrm{LnL}i}^{\mathrm{CF3CO2}}$ and entropic $\Delta S_{\mathrm{LnL}i}^{\mathrm{CF3CO2}}$ contributions to the free energy of formation of the complexes [Ln(**L*i***^{C12})$(CF_3CO_2)_3$] (eq 2) point to an enthalpically driven complexation process in noncoordinating dichloromethane ($\Delta H_{\mathrm{LnL}i}^{\mathrm{CF3CO2}} < 0$, Table 7). The entropic trend, $-T\Delta S_{\mathrm{LnL}i}^{\mathrm{CF3CO2}} > 0$ implies that dissociation is favored at high temperature, a situation which occurs when solid-state samples are heated to form thermotropic liquid crystals. The limited enthalpic stability of the trifluoroacetate complexes is thus expected to be deleterious for the conservation of the molecular

(27) (a) Gampp, H.; Maeder, M.; Meyer, C. J.; Zuberbühler, A. *Talanta* **1985**, *32*, 1133. (b) Gampp, H.; Maeder, M.; Meyer, C. J.; Zuberbühler, A. *Talanta* **1986**, *33*, 943.

Table 6. Auto-Diffusion Coefficients (D in $m^2\ s^{-1}$) Obtained by DOSY-NMR for the Ligands $\mathbf{Li}^{C12}$ and for the Complexes $[Ln(\mathbf{Li}^{C12})(CF_3CO_2)_3]$ ($[\mathbf{Li}^{C12}]_{tot} = [Ln(CF_3CO_2)_3]_{tot} = 10^{-2}$ mol dm^{-3}, i = 3, 4; Ln = Lu, Y, CD_2Cl_2) and Ratios of Molecular Weights Estimated with eq 1

	T (K)	D_{Ligand}	$D_{Complex}$	$D_{Ligand}/D_{Complex}$	$MM_{Ligand}/MM_{Complex}$
$[Lu(\mathbf{L3}^{C12})(CF_3CO_2)_3]$	293	$4.7(1) \times 10^{-10}$	$4.5(1) \times 10^{-10}$	1.04(4)	1.3(2)
$[Y(\mathbf{L3}^{C12})(CF_3CO_2)_3]$	293	$4.7(1) \times 10^{-10}$	$4.4(1) \times 10^{-10}$	1.08(4)	1.5(2)
$[Lu(\mathbf{L4}^{C12})(CF_3CO_2)_3]$	303	$5.2(1) \times 10^{-10}$	$5.1(1) \times 10^{-10}$	1.03(4)	1.3(2)
$[Y(\mathbf{L4}^{C12})(CF_3CO_2)_3]$	293	$4.6(1) \times 10^{-10}$	$4.3(1) \times 10^{-10}$	1.09(4)	1.6(2)

Table 7. Thermodynamic Parameters Obtained for the Formation of the Complexes $[Ln(\mathbf{L3}^{C12})(CF_3CO_2)_3]$, $[Ln(\mathbf{L4}^{C12})(CF_3CO_2)_3]$, and $[Ln(\mathbf{L3}^{C12})(NO_3)_3]$ in Solution

ligand	Ln(III)	anion	solvent	$\log(\beta^X_{LnLi})^a$	ΔH^X_{LnLi} [b]	ΔS^X_{LnLi} [c]	method[d]	ref
$\mathbf{L3}^{C12}$	La	NO_3^-	CH_2Cl_2/CH_3CN (1:1)	5.7(2)			spectro	15
$\mathbf{L3}^{C12}$	Eu	NO_3^-	CH_2Cl_2/CH_3CN (1:1)	5.3(2)			spectro	15
$\mathbf{L3}^{C12}$	Y	NO_3^-	CH_2Cl_2/CH_3CN (1:1)	5.9(1)			spectro	15
$\mathbf{L3}^{C12}$	Lu	NO_3^-	CH_2Cl_2/CH_3CN (1:1)	6.1(1)			spectro	15
$\mathbf{L3}^{C12}$	La	$CF_3CO_2^-$	CH_2Cl_2/CH_3CN (1:1)	4.5(1)			spectro	this work
$\mathbf{L3}^{C12}$	Eu	$CF_3CO_2^-$	CH_2Cl_2/CH_3CN (1:1)	4.6(1)			spectro	this work
$\mathbf{L3}^{C12}$	Y	$CF_3CO_2^-$	CH_2Cl_2/CH_3CN (1:1)	4.6(1)			spectro	this work
$\mathbf{L3}^{C12}$	Lu	$CF_3CO_2^-$	CH_2Cl_2/CH_3CN (1:1)	4.6(1)			spectro	this work
$\mathbf{L3}^{C12}$	Y	$CF_3CO_2^-$	CD_2Cl_2	3.1(2)	−14(7)	10(15)	VT-NMR	this work
$\mathbf{L3}^{C12}$	Lu	$CF_3CO_2^-$	CD_2Cl_2	3.6(2)	−32(7)	−40(15)	VT-NMR	this work
$\mathbf{L4}^{C12}$	Y	$CF_3CO_2^-$	CD_2Cl_2	3.8(2)	−37(7)	−53(15)	VT-NMR	this work
$\mathbf{L4}^{C12}$	Lu	$CF_3CO_2^-$	CD_2Cl_2	4.2(2)	−24(6)	−43(12)	VT-NMR	this work

[a] Given at 293 K for the equilibrium $\mathbf{Li}^{C12} + LnX_3 \rightleftharpoons [Ln(\mathbf{Li}^{C12})X_3]$. [b] Units of kJ mol^{-1}. [c] Units of J mol^{-1} K^{-1}. [d] Spectro stands for spectrophotometric titrations at 293 K. VT-NMR is decomplexation followed by variable-temperature NMR.

structures of the complexes when entering mesophases at high temperature.

Thermal and Mesomorphic Properties of $[Ln(Li^{C12})(CF_3CO_2)_3]$ (1−14). The thermal and mesomorphic properties of complexes **1**−**14** have been investigated by using a combination of thermogravimetric analysis (TGA), differential scanning calorimetry (DSC), polarized light microscopy (PLM), and small-angle X-ray scattering (SAXS). Except for the loss of cocrystallized water molecules in **8** and **13**, TGA shows that the complexes do not decompose prior to isotropization, which occurs around 208−248 °C (Table 8). Isotropization is rapidly followed by decomposition in the liquid phase and natural textures reliable for investigation by PLM cannot be obtained upon cooling from the isotropic liquid. We are thus limited to observe textures (PLM) or to record SAXS profiles on mesophases formed during the heating and cooling processes, which have not reached the critical isotropization temperature.

For the V-shaped complexes $[Ln(\mathbf{L3}^{C12})(CF_3CO_2)_3]$ (**1**−**7**), the DSC traces reveal several Cr → Cr or Cr → AS transitions occurring at low temperature (AS = amorphous solid or conformationally disordered crystal phase), which strongly depend on the mode of isolation of the sample (crystallization, precipitation), followed by a single endotherm at high temperature (225−248 °C) assigned to isotropization by PLM. However, PLM observations also indicate that, for each studied complex, the amorphous solid or conformationally disordered crystal phase transforms into a liquid crystalline phase about 10−20 °C prior to isotropization (Table 8). The observed birefringent textures are poorly developed and cannot be used for the unambiguous assignment of the supramolecular organization in the mesophases. However, the associated SAXS profiles collected at high temperature for Ln = Pr (**1**) and Ln = Sm (**2**) systematically show the collapse of the fine peaks of the crystalline phase to give a few residual, but significant, reflections characteristic of the mesophase (Figure S6, Supporting Information). We also note that some hysteresis occurs during the cooling process, thus allowing the collection of SAXS profiles in the mesophase at temperatures slightly lower than those mentioned for the AS → LC transition in Table 8. However, the scattered peaks recorded in the mesophases are often broad and poorly resolved, and they belong to different species, as deduced after peak-shape analysis, which are diagnostic for the coexistence of different phases or organizations. Consequently, the unambiguous indexation of the reflections is difficult, but we systematically observe a sequence of 4−5 reflections at low angle with squared spacing ratios of $h^2 + k^2 + hk = 1$, 4, 7, 9, and 13 (Table 9), compatible with the formation of a hexagonal columnar arrangement for the major component of the mesophase (Col_h, plane group *p6* or *p6mm*).[14,15] The nonobservation of the reflections corresponding to the squared spacing ratios 3 and 12 are likely the result of the poor quality of the X-ray pattern. The concomitant systematic observation of a broad diffuse band centered at 4.6 Å, characteristic of the molten alkyl chains, confirms the liquidlike nature of the mesophases. The analysis of the X-ray diffraction profiles obtained for $[Pr(\mathbf{L3}^{C12})(CF_3CO_2)_3]$ (**1**) and $[Sm(\mathbf{L3}^{C12})(CF_3CO_2)_3]$ (**2**) leads to an intercolumn separation in the range of a = 40.0−40.7 Å, with associated cross section areas of S = 1383−1432 $Å^2$ (Table 9). The additional broad reflection observed at 5.2 Å is reminiscent of the intermetallic separation measured for the $[La(\mathbf{L3}^{C4})(CF_3CO_2)_3]_2$ dimer in the crystal structure of **17** (4.7955(8) Å). Taking the latter distance as the average separation between two slices within the column ($h \approx 5.2$ Å), we calculate unit cell volumes of $V = Sh$ = 7192 (Ln = Pr) and 7446 $Å^3$ (Ln = Sm). Assuming a realistic density of $d \approx 1$ g cm^{-3} in the mesophase, we eventually estimate with eq 4 that the number of molecules per unit cell in $[Ln(\mathbf{L3}^{C12})(CF_3CO_2)_3]$ amounts to Z = 2 (Ln = Pr, Sm), in agreement with the existence of bridged

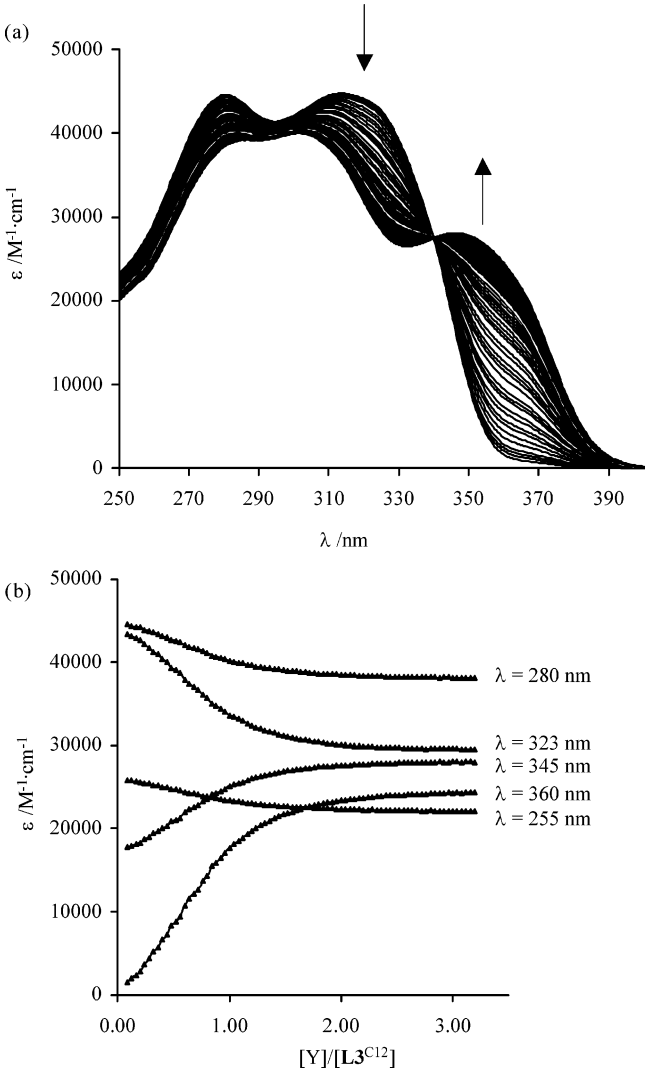

Figure 7. (a) Variation of absorption spectra observed for the spectrophotometric titration of $\mathbf{L3}^{C12}$ (10^{-4} mol dm^{-3} in acetonitrile/dichloromethane (1:1)) with $Y(CF_3CO_2)_3 \cdot 2H_2O$ at 293 K ($Y/\mathbf{L3}^{C12} = 0.1-3.1$) and (b) the corresponding variation of observed molar extinctions at 5 different wavelengths.

disklike dimers packed along the columns (N_{Av} is Avogadro's number, MM_m is the molecular weight of the molecule in g mol^{-1}, and V is the volume of the unit cell in $Å^3$).[15]

$$Z = (dN_{Av}V \times 10^{-24})/MM_m \quad (4)$$

By using the crystal structure of $[La(\mathbf{L3}^{C4})(CF_3CO_2)_3]_2$ as a structural model, a diameter of 20 Å can be estimated for the projection of the rigid organometallic core along the columnar axis (Figure 8). The further connection of dodecyloxychains in their elongated forms (15 Å)[19,20] to the gallic acid residues in $[Ln(\mathbf{L3}^{C12})(CF_3CO_2)_3]_2$, instead of the butyloxy chains found in the model compound $[La(\mathbf{L3}^{C4})(CF_3CO_2)_3]_2$, gives a total diameter of 50 Å, which implies important coiling of the chains or partial interdigitations between the molten alkyl chains in the hexagonal columnar mesophases to fill the available volume. These structural data contrast with the existence of monomeric elliptic hemidisklike nitrato complexes $[Ln(\mathbf{L3}^{C12})(NO_3)_3]$, which are responsible for the formation of related hexagonal columnar mesophases displaying shorter intercolumn separations (a = 31.2−31.9 Å).[15] However, we again stress here that SAXS profiles collected in the temperature range of the mesophases occurrence are complicated and are not easy to analyze because of the coexistence of various molecular species and thus various phases, which points to a likely partial entropically driven dissociation of $[Ln(\mathbf{L3}^{C12})(CF_3CO_2)_3]_2$ occurring at high-temperature according to eq 5. This provides mixtures of mesomorphic complexes together with liquid ligand $\mathbf{L3}^{C12}$ and solid lanthanide salts $[Ln(CF_3CO_2)_3]$. Obviously, the transition temperatures given in Table 8 reflect the behavior of the mixtures.

$$[Ln(\mathbf{L}\textit{i}^{C12})(CF_3CO_2)_3]_2 \rightleftharpoons 2[Ln(\mathbf{L}\textit{i}^{C12})(CF_3CO_2)_3] \rightleftharpoons 2\mathbf{L}\textit{i}^{C12} + 2Ln(CF_3CO_2)_3 \quad (5)$$

For the I-shaped complexes, $[Ln(\mathbf{L4}^{C12})(CF_3CO_2)_3]$ (**8**−**14**), we also detected Cr → LC transitions at high temperature occurring prior to isotropization (Table 8). PLM observations show viscous birefringent textures, typical of liquid-crystalline behaviors. Again, isotropization occurs around 208−245 °C, and it is followed by fast decomposition. Although first-order transitions are detected by DSC for the Cr → LC transition during the first heating process (Table 8), subsequent cooling freezes the organization in the mesophase, and no further endotherm or exotherm can be detected by DSC during subsequent heating/cooling cycles. SAXS reflections are again broad and poorly resolved, and they show lamellar organizations in the mesophase for Ln = Pr (**8**), Ho (**11**), and Yb (**12**). The interlayer separation in the lamellar mesophase amounts to d = 43.5−44.3 Å, and the molecular areas are A = 84−85 $Å^2$ (Table 9), in agreement with related values found in the lamello-columnar mesophases characterized for $[Ln(\mathbf{L4}^{C12})(NO_3)_3]$ (d = 39−41 Å and A = 88−90 $Å^2$).[15] The interlayer separation is indeed smaller than the total length of the coordinated I-shaped ligand in its elongated form (58 Å), estimated from the crystal structure of $[Lu(\mathbf{L5})(CF_3CO_2)_3]_2$,[19] which implies partial chain interdigitation between the layers or chain-coiling to accommodate the large molecular surface area. Such lamellar organization has been found to be diagnostic for the existence of bridged dimers $[Ln(\mathbf{L4}^{C12})(NO_3)_3]_2$ in the mesophase, and we propose a similar behavior for **8**, **11**, and **12**, which are thus assigned to exist as dimers $[Ln(\mathbf{L4}^{C12})(CF_3CO_2)_3]_2$ in the lamellar phase.

Altogether, these thermal, PLM, and crystallographic data show that the trifluoroacetate complexes $[Ln(\mathbf{L}\textit{i}^{C12})(CF_3CO_2)_3]$ display liquid-crystalline behaviors at high temperature. The poor quality of the birefringent textures and of the associated SAXS pattern strongly suggests that, depending on the lanthanide and on the shape of the ligand, the two successive entropically driven equilibria illustrated in eq 5 produce mixtures of complexes, ligands, and lanthanide salts at high temperature, a process which is deleterious for deducing precise structural correlations between molecular shapes and mesoscopic organizations. Nevertheless, the interpretation of the SAXS profiles suggests that the dimeric units of $[Ln(\mathbf{L}\textit{i}^{C12})(CF_3CO_2)_3]_2$ are the major component of

Table 8. Phase-Transition Temperatures and Associated Thermodynamic Parameters Observed by DSC, PLM, and Thermogravimetric Analyses for the Complexes [Ln(**L3**^{C12})$(CF_3CO_2)_3$] (**1**−**7**) and [Ln(**L4**^{C12})$(CF_3CO_2)_3]\cdot n H_2O$ (**8**−**14**)

	transition[a]	T (°C)[b]	ΔH (kJ mol^{-1})	ΔS (J mol^{-1} K^{-1})	weight loss (%)	decomp
[Pr(**L3**^{C12})$(CF_3CO_2)_3$] (**1**)	$Cr^1 \rightarrow$ AS	102	4.8	13	0	240
	AS $\rightarrow Col_h$	220	*c*	*c*		
	$Col_h \rightarrow$ I	227		73		
[Sm(**L3**^{C12})$(CF_3CO_2)_3$] (**2**)	$Cr^1 \rightarrow$ AS	37	45	146	0	250
	AS $\rightarrow Col_h$	220	*c*	*c*		
	$Col_h \rightarrow$ I	240	50	97		
[Gd(**L3**^{C12})$(CF_3CO_2)_3$] (**3**)	$Cr^1 \rightarrow$ AS	38	38.7	124	0	260
	AS $\rightarrow Col_h$	225	*c*	*c*		
	$Col_h \rightarrow$ I	248	48.7	93.4		
[Ho(1**L3**^{C12})$(CF_3CO_2)_3$] **(4)**	$Cr^1 \rightarrow Cr^2$	37	18.6	53.8	0	261
	$Cr^2 \rightarrow$ AS	151	6.26	14.6		
	AS $\rightarrow Col_h$	230	*c*	*c*		
	$Col_h \rightarrow$ I	247	62	119		
[Yb(**L3**^{C12})$(CF_3CO_2)_3$] (**5**)	AS $\rightarrow$ LC	219	*c*	*c*	0	265
	LC $\rightarrow$ I	234	78	134		
[Lu(**L3**^{C12})$(CF_3CO_2)_3$] (**6**)	$Cr^1 \rightarrow Cr^2$	33	0.5	1.5	0	265
	$Cr^2 \rightarrow$ AS	45	0.4	1.3		
	AS $\rightarrow$ LC	210	*c*	*c*		
	LC $\rightarrow$ I	225	56.6	113.6		
[Y(**L3**^{C12})$(CF_3CO_2)_3$] (**7**)	$Cr^1 \rightarrow$ AS	37	*d*	*d*	0	255
	AS $\rightarrow$ LC	230	*c*	*c*		
	LC $\rightarrow$ I	245	*d*	*d*		
[Pr(**L4**^{C12})$(CF_3CO_2)_3]\cdot 2.5H_2O$ (**8**)	$Cr^1 \rightarrow Cr^2$	15	13	45.6	1.77	250
	$Cr^2 \rightarrow Cr^3$	37	7.8	25	(2.2 H_2O)	
	$Cr^3 \rightarrow Cr^4$	56	21.4	55.6		
	Cr4 $\rightarrow$ lamellar	215	22.7	46		
	lamellar $\rightarrow$ I	245	*e*	*e*		
[Sm(**L4**^{C12})$(CF_3CO_2)_3$] (**9**)	$Cr^1 \rightarrow Cr^2$	56	18	55	0	260
	$Cr^2 \rightarrow$ lamellar	219	24	48		
	lamellar $\rightarrow$ I	226	10	20		
[Gd(**L4**^{C12})$(CF_3CO_2)_3$] (**10**)	$Cr^1 \rightarrow Cr^2$	16	38	131	0	270
	$Cr^2 \rightarrow Cr^3$	34	20	64		
	$Cr^3 \rightarrow$ lamellar	213	23.5	48		
	lamellar $\rightarrow$ I	236	24.3	47		
[Ho(**L4**^{C12})$(CF_3CO_2)_3$] (**11**)	Cr $\rightarrow$ lamellar	155	22	51.7	0	>260
	lamellar $\rightarrow$ I	216	13.4	27.4		
[Yb(**L4**^{C12})$(CF_3CO_2)_3$] (**12**)	Cr $\rightarrow$ lamellar	189	25.4	55	0	270
	lamellar $\rightarrow$ I	235	23.9	47		
[Lu(**L4**^{C12})$(CF_3CO_2)_3]\cdot 0.5H_2O$ (**13**)	Cr $\rightarrow$ LC	92	37.6	103	0.69	250
	LC $\rightarrow$ I	208	14.8	31	(0.8 H_2O)	
[Y(**L4**^{C12})$(CF_3CO_2)_3$] (**14**)	$Cr^1 \rightarrow Cr^2$	42	4.8	15.3	0	270
	$Cr^2 \rightarrow$ lamellar	184	19.1	42		
	lamellar $\rightarrow$ I	240	25.8	50		

[a] Cr = crystal, AS = amorphous solid or conformationally disordered crystal phase, LC = liquid crystalline phase, I = isotropic fluid. Enthalpic and entropic changes are obtained by DSC. [b] Temperature is given for the first heating process (see text). [c] Phase transition assessed by PLM and SAXS measurements. [d] Values of ΔH and ΔS were not fully reproducible. [e] Masked by decomposition.

the mixtures in the mesophase, which contrasts with the existence of monometallic hemidisklike complexes as the major component of the liquid-crystalline material for the nitrato complexes [Ln(**L*i***^{C12})$(NO_3)_3$].[15]

Conclusion

Contrary to our initial assumption claiming that nitrates in [Ln(**L*i***^{C12})$(NO_3)_3$] can be replaced with trifluoroacetetate in [Ln(**L*i***^{C12})$(CF_3CO_2)_3$] without affecting the metallic coordination spheres, except for an improved trend toward dimerization, the present results show that [Ln$(NO_3)_3$] and [Ln$(CF_3CO_2)_3$] behave quite differently toward neutral aromatic tridentate nitrogen ligands. Crystal structures collected on nonlipophilic models indicate that the Ln−N bond distances increase by ∼0.1 Å in the trifluoroacetate complexes, which is diagnostic for a reduced Ln−ligand interaction. This trend is confirmed by thermodynamic data recorded in poorly coordinating solvents, which strongly limits the thermal stabilities of these complexes at high temperature. Although we are aware that the thermodynamic parameters of the complexation process (eq 2) are different when solid state or solution samples are considered, the observation in noncoordinating dichloromethane solutions of an enthalpically driven process ($\Delta H_{LnLi}^{CF3CO2} < 0$), which can be balanced at high temperature by the entropic term ($-T\Delta S_{LnLi}^{CF3CO2} > 0$), is a strong support for related processes occurring in the mesophases, in which solvent is excluded. In this context, the detection of mesophases at high temperature within a narrow range for [Ln(**L*i***^{C12})$(CF_3CO_2)_3$] suggests the existence of mixtures (complexes, dissociated ligands, and metal salts), which are responsible for the limited accuracy of the SAXS patterns. However, the analysis of residual organizations in the mesophases indicates that the dimeric disklike units [Ln(**L3**^{C12})$(CF_3CO_2)_3]_2$ correspond to the major component in the mesophases, while hemidisklike monomers dominate the composition of the mesophases for

Table 9. Indexation at a Given Temperature (T (°C)) for the Reflections Detected in the Liquid-Crystalline Phases by SAXS for the Complexes [Ln(**L3**^{C12})$(CF_3CO_2)_3$] (Ln = Pr (**1**), Sm (**2**)) and [Ln(**L4**^{C12})$(CF_3CO_2)_3$] (Ln = Pr (**8**), Ho (**11**), Yb (**12**))[a]

Pr(**L3**^{C12})$(CF_3CO_2)_3$

T (°C)	$d_{hk(mes)}$ (Å)	I (au)	h^2+k^2+hk	hk	$d_{hk(calcd)}$ (Å)	
220	34.70	VS	1	10	34.60	$a = 40.0$ Å
heating	17.45	M	4	20	17.30	$S = 1383$ Å^2
	13.04	W	7	21	13.08	Col_h
	11.55	W	9	30	11.53	
	9.58	VW	13	31	9.60	
	5.2	VW				
	4.6	Br				

Sm(**L3**^{C12})$(CF_3CO_2)_3$

T (°C)	$d_{hk(mes)}$ (Å)	I (au)	h^2+k^2+hk	hk	$d_{hk(calcd)}$ (Å)	
220	35.50	VS	1	10	35.21	$a = 40.7$Å
heating	17.96	M	4	20	17.61	$S = 1432$ Å^2
	13.01	W	7	21	13.31	Col_h
	11.82	W	9	30	11.74	
	5.2	VW				
	4.6	Br				

Pr(**L4**^{C12})$(CF_3CO_2)_3$

T (°C)	$d_{hkl(mes)}$ (Å)	I (au)	h^2+k^2+hk	hkl	$d_{hkl(calcd)}$ (Å)	
205	43.76	S		001	44.25	lamellar
heating	22.20	VW		002	22.12	$A = 84.0$ Å^2
	4.6	Br				

Ho(**L4**^{C12})$(CF_3CO_2)_3$

T (°C)	$d_{hkl(mes)}$ (Å)	I (au)	h^2+k^2+hk	hkl	$d_{hkl(calcd)}$ (Å)	
180	43.51	S		001	43.48	lamellar
heating	21.70	VW		002	21.74	$A = 84.7$ Å^2
	4.6	Br				

Yb(**L4**^{C12})$(CF_3CO_2)_3$

T (°C)	$d_{hkl(mes)}$ (Å)	I (au)	h^2+k^2+hk	hkl	$d_{hkl(calcd)}$ (Å)	
210	43.51	VS		001	43.86	lamellar
heating	21.82	M		002	21.93	$A = 85.0$ Å^2
	4.6	Br				

[a] d_{mes} and d_{calcd} are the measured and calculated diffraction spacing, a is the lattice parameter, $S = a\sqrt{3}/2$ is the cross section of the column, $A = V_{mol}/\langle d_{001}\rangle = MM/(dN_{Av} \times 10^{-24}) \times 1/\langle d_{001}\rangle$ is the molecular area for the lamellar phase (d is the density in the mesophase and is ~1 g cm^{-3}, MM is the molecular mass of the complex in g mol^{-1}, and N_{Av} is Avogadro's number). I refers to the intensity of the reflection (VS, very strong; S, strong; W, weak; VW, very weak; Br, broad).

the nitrato complexes [Ln(**L3**^{C12})$(NO_3)_3$].[15] Conversely, similar behaviors are obtained for the complexes [Ln(**L4**^{C12})$(CF_3CO_2)_3$] and [Ln(**L4**^{C12})$(NO_3)_3$] with the observation of lamellar organizations associated with the existence of rodlike dimeric units [Ln(**L4**^{C12})$(X)_3]_2$ (X = $CF_3CO_2^-$, NO_3^-). These conclusions agree with the crystal structures of the model complexes, for which trifluoroacetato-bridged dimers are systematically observed in the absence of additional water molecules, and with the crystal structures of $Ln(NO_3)_3 \cdot xH_2O$[28] and $Ln(CF_3CO_3)_3 \cdot xH_2O$,[21b] which display monometallic and bridged-polymetallic structural patterns, respectively. If we now focus on our search for inducing smectic or nematic lanthanide-containing mesophases with

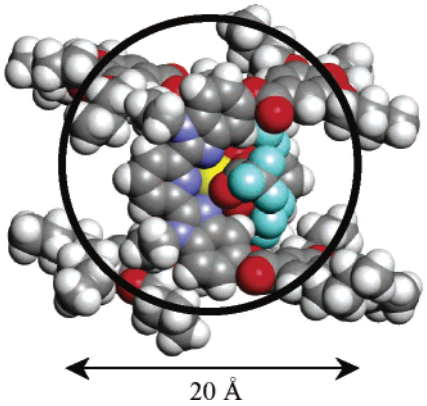

Figure 8. CPK view of the molecular structure of [La(**L3**^{C4})$(CF_3CO_2)_3]_2$ along the La−La direction showing the circular projection of the rigid organometallic core.

hexacatenar ligands, the replacement of NO_3^- with $CF_3CO_2^-$ is disappointing, but it taught us that (i) the stability of the Ln−ligand bonds can be modulated by the coordinated counteranions, (ii) $CF_3CO_2^-$ interacts slightly stronger with Ln(III) than does NO_3^-, and (iii) increased Ln−Ligand interactions (and associated larger enthalpically driven resistance to entropic dissociation at high temperature) may be implemented by using counteranions which display weaker interactions with Ln(III). In this context, we are currently focusing our efforts on the use of trifluoromethanesulfonates, halides, and pseudo-halides, which are known to match the latter criteria.[29]

Experimental Section

Solvents and Starting Materials. These were purchased from Fluka AG (Buchs, Switzerland) and Aldrich and were used without further purification unless otherwise stated. The ligands **L3**^{C12} and **L4**^{C12} were prepared according to literature procedures.[15] The trifluoroacatate salts, $Ln(CF_3CO_2)_3 \cdot xH_2O$ (Ln = La−Lu, Y; x = 1−4), were prepared from the corresponding oxides (Rhodia, 99.99%).[30] The Ln content of the solid salts was determined by complexometric titrations with Titriplex III (Merck) in the presence of urotropine and xylene orange.[31] Acetonitrile and dichloromethane were distilled over calcium hydride.

Preparation of the [Ln(L*i*^{C12})$(CF_3CO_2)_3$] (*i* = 3, 4; Ln = Pr, Sm, Gd, Ho, Yb, Lu, Y; 1−14) Complexes. **L3**^{C12} or **L4**^{C12} (5.84×10^{-5} mol) in dichloromethane (5 mL) was added to $Ln(CF_3CO_2)_3 \cdot xH_2O$ (Ln = Pr, Sm, Gd, Ho, Yb, Lu, Y; x = 2−4) in acetonitrile (5 mL). After the mixture was stirred for 1 h at room temperature, the solvent was evaporated, and the white precipitate was crystallized from pure dichloromethane (−30 °C) to give microscrystalline powders (80−95%), whose elemental analyses (Table S1, Supporting Information) correspond to [Ln(**L3**^{C12})$(CF_3CO_2)_3$] (Ln = Pr (**1**), Sm (**2**), Gd (**3**), Ho (**4**), Yb (**5**), Lu (**6**), Y (**7**)) and [Ln(**L4**^{C12})$(CF_3CO_2)_3] \cdot nH_2O$ (Ln = Pr, n = 2.5 (**8**); Ln = Sm, n = 0 (**9**); Ln = Gd, n = 0 (**10**); Ln = Ho, n = 0 (**11**); Ln = Yb, n = 0 (**12**); Ln = Lu, n = 0.5 (**13**); Ln = Y, n = 0 (**14**)).

(28) Junk, P. C.; Kepert, D. L.; Skelton, B. W.; White, A. H. *Aust. J. Chem.* **1999**, *52*, 497.

(29) Bünzli, J.-C. G.; Milicic-Tang, A. In *Handbook on the Physics and Chemistry of Rare Earths*; Gschneidner, K. A., Eyring, L., Eds.; Elsevier: Amsterdam, 1995; Vol. 21, Chapter 145, p 305.

(30) Desreux, J.-F. In *Lanthanide Probes in Life, Chemical and Earth Sciences*; Bünzli, J.-C. G., Choppin, G. R., Eds.; Elsevier Publishing Co: Amsterdam, 1989; Chapter 2, p 43.

(31) Schwarzenbach, G. *Complexometric Titrations*; Chapman & Hall: London, 1957; p 8.

Table 10. Summary of Crystal Data, Intensity Measurements, and Structural Refinement for $[Lu(\mathbf{L4}^{C0})(CF_3CO_2)_3]_2$ (**15**), $[Lu(\mathbf{L4}^{C0})(CF_3CO_2)_3(H_2O)]\cdot 0.3H_2O$ (**16**), and $[La(\mathbf{L3}^{C4})(CF_3CO_2)_3]_2$ (**17**)

	15	**16**	**17**
formula	$C_{86}H_{58}F_{18}Lu_2N_{10}O_{20}$	$C_{43}H_{31.6}F_9LuN_5O_{11.3}$	$C_{134}H_{154}F_{18}La_2N_{10}O_{32}$
fw	2243.4	1145.1	3036.5
cryst syst	triclinic	triclinic	monoclinic
space group	$P\bar{1}$	$P\bar{1}$	$P2_1/c$
a (Å)	13.1421(12)	12.8253(11)	21.0157(13)
b (Å)	13.2006(9)	13.7314(10)	15.7864(11)
c (Å)	13.2886(11)	14.5785(10)	24.2601(13)
α (deg)	90.227(9)	90.854(9)	90
β (deg)	109.452(9)	115.333(9)	114.098(7)
γ (deg)	100.751(10)	107.074(9)	90
V (Å^3)	2130.2(3)	2188.6(4)	7347.1(9)
Z	1	2	2
cryst size (mm)	0.06 × 0.164 × 0.185	0.08 × 0.13 × 0.18	0.14 × 0.27 × 0.44
d_{calcd} (Mg m^{-3})	1.749	1.738	1.373
μ(Mo Kα) (mm^{-1})	2.422	2.362	0.670
T_{min}, T_{max}	0.5389, 0.8789	0.6912, 0.8763	0.8113, 0.9102
2θ max (deg)	56.0	53.4	51.6
no. of reflns collected	27979	25885	77870
no. of independent reflns	9527	8794	14101
criterion (q) for obsd reflns[a,b]	4	4	3
no. of obsd[a] (used[b]) reflns	6665 (6872)	6623 (6798)	6416 (6823)
no. of variables	637	638	792
weighting scheme (p)[c]	0.00015	0.0001	0.0002
max and min $\Delta\rho$ (e Å^{-3})	1.28, −0.84	1.10, −1.00	1.67, −1.12
Flack param (x)			
GOF(F)[d] (all data)	1.011(9)	1.11(1)	1.73(1)
R,[e] R_w[f]	0.030, 0.029	0.026, 0.025	0.062, 0.063

[a] $|F_o| > q\sigma(F_o)$. [b] Used in the refinements (including reflns with $|F_o| \le q\sigma(F_o)$ if $|F_c| > |F_o|$). [c] $w = 1/[\sigma^2(F_o) + p(F_o)^2]$. [d] $S = [\sum\{((F_o - F_c)/\sigma(F_o))^2\}/(N_{ref} - N_{var})]^{1/2}$. [e] $R = \sum||F_o| - |F_c||/\sum|F_o|$. [f] $R_w = [\sum(w|F_o| - |F_c|)^2/\sum w|F_o|^2]^{1/2}$.

Single-Crystal Structure Determinations of $[Lu(\mathbf{L4}^{C0})(CF_3CO_2)_3]_2$ (15), $[Lu(\mathbf{L4}^{C0})(CF_3CO_2)_3(H_2O)]\cdot 0.3H_2O$ (16), and $[La(\mathbf{L3}^{C4})(CF_3CO_2)_3]_2$ (17). A summary of crystal data, intensity measurements, and structure refinements is collected in Table 10. All crystals were mounted on quartz fibers with protection oil. Cell dimensions and intensities were measured at 200 K on a Stoe IPDS diffractometer with graphite-monochromated Mo Kα radiation (λ = 0.71073 Å). Data were corrected for Lorentz and polarization effects and for absorption. The structures were solved by direct methods (SIR97);[32] all other calculation were performed with the XTAL[33] system and ORTEP[34] programs.

Comments on the Crystal Structure of 15. The disordered CF_3 groups of the trifluoroacetate anions a and b were each refined on two sites with population parameters 0.7 (using U_{aniso}) and 0.3 (using U_{iso}). The atomic positions of the hydrogen atoms were calculated.

Comments on the Crystal Structure of 16. The disordered CF_3 group of the trifluoroacetate anion a was refined with restraints on bond lengths and bond angles on two sites with population parameters 0.65 (using U_{aniso}) and 0.35 (using U_{iso}). The noncoordinate water molecule O2w was refined with a population parameter of 0.3 (using U_{iso}). The atomic positions of the hydrogen atoms were calculated, except for the hydrogen atoms of the coordinated water molecule O1w, which were observed and refined with restraints on bond lengths and bond angles and blocked during the last cycles.

Comments on the Crystal Structure of 17. The preparation of monocrystals with the coordinated V-shaped ligand $\mathbf{L3}^{Cn}$ were extremely difficult, and only data collections for the $[La(\mathbf{L3}^{C4})(CF_3CO_2)_3]_2$ (**17**) complex were of sufficient (but still limited) quality for being considered for refinements. The disordered trifluoroacetate c was distributed over two positions, one corresponding to a monodentate binding mode (population parameter 0.4, U_{iso}) and the second displaying a bidentate binding mode (population parameter 0.6, U_{iso}, Figure S5, Supporting Information). The disordered CF_3 group of the trifluoroacetate anion b was refined on two sites with population parameters 0.5 (using U_{aniso}). The ethyl substituents of the benzimidazole rings were refined with isotropic displacement parameters. The three butyloxy residues connected to the phenyl ring C14−C19 were disordered, and each was refined with isotropic displacement parameters on two sites with population parameters 0.6 (standard numbering in Figure S7) and 0.4 (primed numbering in Figure S7). The three butyloxy residues connected to the phenyl ring C28−C33 displayed rather large atomic displacement parameters (refined with U_{iso}) but did not show specific disorder. U_{iso} values for C38′, C39′, and C57 were fixed to 0.35 Å^2 because they produced instabilities during the refinements. The atomic positions of the hydrogen atoms were calculated, and all butyloxy chains and trifluoroacetate anions were refined with restraints on bond lengths and bond angles (127 restraints) but with no restriction on torsion angles.

Spectroscopic and Analytical Measurements. UV−vis electronic spectra were recorded at 20 °C from solutions in CH_3CN/CH_2Cl_2 (1:1) with a Perkin-Elmer Lambda 900 spectrometer using quartz cells of 0.1 and 1 mm path lengths. Spectrophotometric titrations were performed with a J&M diode array spectrometer (Tidas series) connected to an external computer. In a typical experiment, 50 mL of $\mathbf{L3}^{C12}$ in CH_3CN/CH_2Cl_2 (1:1) (2×10^{-4} mol dm^{-3}) were titrated at 20 °C with a solution of $Ln(CF_3CO_2)_3\cdot xH_2O$ (10^{-3} mol dm^{-3}) in the same solvent under an inert atmosphere. After each addition of 0.10 mL, the absorbance was recorded using Hellma optrodes (optical path length 0.1 cm)

(32) Altomare, A.; Burla, M. C.; Camalli, M.; Cascarano, G.; Giacovazzo, C.; Guagliardi, A.; Moliterni, G.; Polidori, G.; Spagna, R. *J. Appl. Crystallogr.* **1999**, *32*, 115.
(33) *XTAL 3.2 User's Manual*; Hall, S. R., Flack, H. D., Stewart, J. M., Eds.; Universities of Western Australia and Maryland: Perth, Australia, and College Park, MD,1989.
(34) Johnson, C. K. *ORTEP II*; Report ORNL-5138; Oak Ridge National Laboratory: Oak Ridge, TN, 1976.

immersed in the thermostated titration vessel and connected to the spectrometer. Mathematical treatment of the spectrophotometric data was performed with factor analysis[35] and with the SPECFIT program.[27] ^{1}H NMR spectra were recorded at 25 °C on a Bruker Avance 400 MHz. Chemical shifts are given in ppm with respect to TMS. Diffusion experiments were recorded at a 400 MHz proton−Larmor frequency at room temperature. The sequence corresponds to Bruker pulse program *ledbpgp2s*[36] using stimulated echo, bipolar gradients, and longitudinal eddy current delay as a z filter. The four 2 ms gradient pulses have sine-bell shapes and amplitudes ranging linearly from 2.5 to 50 G/cm in 16 steps. The diffusion delay was 100 ms, and the number of scans was 16. The processing was done using a line broadening of 5 Hz and the diffusion rates calculated using the Bruker processing package. TG studies were performed with a thermogravimetric balance Seiko TG/DTA 320 (under N_2). DSC traces were obtained with a Seiko DSC 220C differential scanning calorimeter from 3 to 5 mg samples (5 °C min^{-1}, under N_2). The characterization of the mesophases were performed with a Leitz Orthoplan-Pol polarizing microscope with a Leitz LL 20×/0.40 polarizing objective, equipped with a Linkam THMS 600 variable-temperature stage. The SAXS patterns were obtained with two different experimental setups, and in all cases, the crude powder was filled in Lindemann capillaries of 1 mm diameter. The characterization of the wide-angle region and the measurements of the periodicities was achieved using a linear monochromatic Cu Kα_1 beam obtained with a sealed-tube generator (900 W) and a bent quartz monochromator. One set of diffraction patterns was registered with a curved counter Inel CPS 120, for which the sample temperature was controlled within ±0.05 °C; periodicities up to 60 Å could be measured. The other set of diffraction patterns was registered on Image Plate; the cell parameters were calculated from the position of the reflection at the smallest Bragg angle, which was in all cases the most intense. Periodicities up to 90 Å could be measured, and the sample temperature was controlled within ±0.3°C. The exposure times were varied from 1 to 24 h depending on the specific reflections being sought (weaker reflections obviously taking longer exposure times). Elemental analyses were performed by Dr. H. Eder from the microchemical Laboratory of the University of Geneva.

Acknowledgment. This work is supported through grants from the Swiss National Science Foundation. We thank Ms. A. Marechal for technical support.

Supporting Information Available: Tables of elemental analyses (Table S1) and least-squares plane data (Tables S2−S4), crystallographic data in CIF format for complexes **15**−**17**, VT-^{1}H NMR data for complex [Ln(**Li**^{C12})(CF$_3$CO$_2$)$_3$] (Tables S5−S8), and figures showing optimized superimpositions of molecular structures (Figures S1 and S2), stereoviews of the unit cells in **15** and **16** (Figures S3 and S4), XRD patterns of [Sm(**L3**^{C12})(CF$_3$CO$_2$)$_3$] (Figure S6), and complementary views of the crystal structure of **17** (Figures S5 and S7). This material is available free of charge via the Internet at http://pubs.acs.org. CCDC-286529, CCDC-286531, and CCDC-286530 contain the supplementary crystallographic data for **15**, **16**, and **17** respectively. The CIF files can be obtained free of charge via www.ccdc.cam.ac.uk/conts/retrieving.html (or from the Cambridge Crystallographic Data Centre, 12 Union Road, Cambridge CB2 1EZ, U.K.; fax (+ 44) 1223-336-033; or deposit@ccdc.cam.ac.uk).

IC052017U

(35) Malinowski, E. R.; Howery, D. G. *Factor Analysis in Chemistry*; Wiley: New York, 1980.
(36) Wu, D.; Chen, A.; Johnson, C. S., Jr. *J. Magn. Reson. A* **1995**, *155*, 260.